Monthly Notices of the ROYAL ASTRONOMICAL SOCIETY

MNRAS **497,** 747–764 (2020)
Advance Access publication 2020 July 6

doi:10.1093/mnras/staa1923

The formation times and building blocks of Milky Way-mass galaxies in the FIRE simulations

Isaiah B. Santistevan,[1★] Andrew Wetzel [1] Kareem El-Badry [2] Joss Bland-Hawthorn [3,4] Michael Boylan-Kolchin [5] Jeremy Bailin,[6] Claude-André Faucher-Giguère [7] and Samantha Benincasa [1]

[1]Department of Physics & Astronomy, University of California, Davis, CA 95616, USA
[2]Department of Astronomy, Theoretical Astrophysics Center, University of California Berkeley, Berkeley, CA 94720, USA
[3]Sydney Institute for Astronomy, School of Physics A28, University of Sydney, Sydney, NSW 2006, Australia
[4]ARC Centre of Excellence in All Sky Astrophysics in Three Dimensions (ASTRO-3D), Sydney, NSW 2006, Australia
[5]Department of Astronomy, The University of Texas at Austin, 2515 Speedway, Stop C1400, Austin, TX 78712-1205, USA
[6]Department of Physics and Astronomy, University of Alabama, Box 870324, Tuscaloosa, AL 35487-0324, USA
[7]Department of Physics and Astronomy and CIERA, Northwestern University, 2145 Sheridan Road, Evanston, IL 60208, USA

Accepted 2020 June 24. Received 2020 June 22; in original form 2020 January 9

ABSTRACT

Surveys of the Milky Way (MW) and M31 enable detailed studies of stellar populations across ages and metallicities, with the goal of reconstructing formation histories across cosmic time. These surveys motivate key questions for galactic archaeology in a cosmological context: When did the main progenitor of an MW/M31-mass galaxy form, and what were the galactic building blocks that formed it? We investigate the formation times and progenitor galaxies of MW/M31-mass galaxies using the Feedback In Realistic Environments-2 cosmological simulations, including six isolated MW/M31-mass galaxies and six galaxies in Local Group (LG)-like pairs at $z = 0$. We examine main progenitor 'formation' based on two metrics: (1) transition from primarily *ex-situ* to *in-situ* stellar mass growth and (2) mass dominance compared to other progenitors. We find that the main progenitor of an MW/M31-mass galaxy emerged typically at $z \sim 3$–4 (11.6–12.2 Gyr ago), while stars in the bulge region (inner 2 kpc) at $z = 0$ formed primarily in a single main progenitor at $z \lesssim 5$ ($\lesssim$12.6 Gyr ago). Compared with isolated hosts, the main progenitors of LG-like paired hosts emerged significantly earlier ($\Delta z \sim 2$, $\Delta t \sim 1.6$ Gyr), with $\sim 4\times$ higher stellar mass at all $z \gtrsim 4$ ($\gtrsim$12.2 Gyr ago). This highlights the importance of environment in MW/M31-mass galaxy formation, especially at early times. On average, about 100 galaxies with $M_{\rm star} \gtrsim 10^5$ $M_\odot$ went into building a typical MW/M31-mass system. Thus, surviving satellites represent a highly incomplete census (by $\sim 5\times$) of the progenitor population.

Key words: galaxies: formation – galaxies: general.

1 INTRODUCTION

The properties of stellar populations within a galaxy, including their age, elemental abundances, and kinematics, all provide rich insight into the galaxy's formation history. For example, early studies of the kinematics of stars with highly radial orbits in the Milky Way (MW) suggested that these stars must have formed differently from those on more disc-like orbits, implying that the MW formed via a gravitational collapse (Eggen, Lynden-Bell & Sandage 1962). Other early studies proposed that stars and clusters in the outer halo formed from material in proto-galaxies that continued to fall into the galaxy after the central regions already collapsed (e.g. Ostriker & Tremaine 1975; Searle & Zinn 1978). We know today that the processes involved in galaxy formation are more elaborate (Freeman & Bland-Hawthorn 2002).

Initial theories for galaxy formation invoked the dissipational collapse of gas in dark-matter (DM) haloes (e.g. Rees & Ostriker 1977; White & Rees 1978; Fall & Efstathiou 1980; Mo, Mao & White 1998). More recent works have examined the effects of galaxy mergers as well (e.g. Springel & Hernquist 2005; Robertson et al. 2006; Stewart et al. 2008; Garrison-Kimmel et al. 2018). In gas-rich mergers, stellar feedback plays an important role in retaining gas content prior to the merger as it can heat the interstellar medium (ISM) and redistribute gas throughout the galaxy, even to larger radii where the effects of gravitational torquing are not as strong (Hopkins 2009). Without feedback, the gas easily is torqued and falls to the centre of the gravitational well, where it gets consumed in a starburst. This implies that some part of galactic discs must survive a merger process, and the thick disc of the MW likely survived a significant merging event, which could have deposited fresh gas into the MW and dynamically heated stars from the thick disc into the stellar halo (Gallart et al. 2019).

The stellar halo of the MW is perhaps the best place to probe the remnants of its early formation process. Various works have studied hierarchical formation of the stellar halo (e.g. Bullock, Kravtsov & Weinberg 2001; Bullock & Johnston 2005; Helmi 2008; Johnston et al. 2008; Cooper et al. 2010; Deason, Mao & Wechsler 2016),

★ E-mail: ibsantistevan@ucdavis.edu

Published by Oxford University Press on behalf of the Royal Astronomical Society

showing that it occurs via the tidal disruption and accretion of many satellite dwarf galaxies. For instance, using cosmological zoom-in simulations, Deason et al. (2016) find that typically 1–2 satellite galaxies contribute most of the accreted stellar material to a stellar halo. More generally, they find that the majority of accreted metal-poor stars come primarily from 'classical' dwarf galaxies (∼40–80 per cent) as opposed to 'ultra-faint' dwarf galaxies (only ∼2–5 per cent). They also find a relation between the galaxy's progenitor mass and its satellite population at $z = 0$: Galaxies with less massive progenitors tend to have more quiescent histories, as well as a less massive surviving satellite population, when compared to the more massive galaxies. Similarly, examining the AURIGA simulations, Monachesi et al. (2019) find a correlation with the number of 'significant progenitors' (the number of progenitors that contribute 90 per cent of the stellar halo mass) and the accreted mass in the halo, with more massive haloes accreting smaller numbers of significant progenitors. Studies of kinematically coherent structures in the MW's halo, like the Sagittarius stream (Newberg et al. 2002; Majewski et al. 2003) and Gaia-Enceladus (Belokurov et al. 2018; Helmi et al. 2018), clearly confirm this hierarchical formation scenario. In particular, Gaia-Enceladus is thought to be comparable in stellar mass to the SMC ($\sim 6 \times 10^8$ M$_\odot$), contributing most of the stars in the (inner) stellar halo (Helmi et al. 2018).

Studies of old and/or metal-poor stars provide the best window into the early formation of the MW (e.g. Scannapieco et al. 2006; Brook et al. 2007; Deason et al. 2016; Griffen et al. 2018; Chiaki & Wise 2019; Sestito et al. 2019). Current spectroscopic surveys (e.g. RAVE, GALAH, APOGEE, and LAMOST) now provide elemental abundances and ages for stars across the MW (e.g. Steinmetz et al. 2006; De Silva et al. 2015; Li et al. 2015; Majewski et al. 2017). These surveys achieve high spectral resolution (up to $R \sim 30\,000$) and signal-to-noise (up to S/N > 100), and are capable of observing stars with [Fe/H] < −2. Recently, the *Pristine* survey has observed significant populations of stars at [Fe/H] < −3, with promise of reaching to [Fe/H] < −4 (Starkenburg et al. 2017b). Interestingly, using observations of metal-poor stars, Sestito et al. (2019) found that a significant fraction of these stars with [Fe/H] < −4 are on disc-like orbits in the MW. Similar work using metal-poor stars from LAMOST also has proven useful in finding halo structures (e.g. Yuan et al. 2019). A key question is where these metal-poor stars come from. Did they form within the MW or did they form in other dwarf galaxies that subsequently merged in? If the latter, it would not make sense to say that they formed in the MW, or at least, its main progenitor.

Recently, using the FIRE-2 (Feedback In Realistic Environments) cosmological zoom-in baryonic simulations, El-Badry et al. (2018b) predicted that the oldest ($z_{\rm form} > 5$), metal-poor stars ([Fe/H] $\lesssim -2$) in the MW should be less centrally concentrated than stars that formed later, because (1) early merger events deposited stars that formed in dwarf galaxies on dispersion-supported orbits, and (2) stars that formed within the primary galaxy were heated to larger orbits via feedback-driven time-varying galactic potential. A similar study by Starkenburg et al. (2017a) found comparable results in the APOSTLE simulations of MW/M31-like pairs for stars with $z_{\rm form} > 6.9$ and [Fe/H] $\lesssim -2.5$.

While current MW surveys give us detailed information about a star's position, kinematics, and elemental abundances, obtaining precise ages for stars remains challenging. Current methods include fitting isochrones to stellar populations in colour–magnitude diagrams, studying oscillation modes of individual stars (astroseismology), using the rotation–age relation to infer ages (gyrochronology), and using detailed elemental abundances (e.g. Chaplin et al. 2014; Martig et al. 2016; Creevey et al. 2017; Silva Aguirre et al. 2018). Uncertainties in the ages of stars using the latter method can be as large as 40 per cent, but this improves if one can use a combination of methods (e.g. Miglio et al. 2017). *Gaia*'s second data release (Gaia Collaboration 2018) now provides distance measurements for over 1.3 billion stars in the MW, allowing astronomers to measure isochrone ages. For example, Gallart et al. (2019) suggest that the MW halo formed 50 per cent of its stars by $z \sim 4.2$ (12.3 Gyr ago) and the thick disc formed 50 per cent by $z \sim 2$ (10.5 Gyr ago). Other analyses reported formation lookback times of the halo of 8–13 Gyr (e.g. Schuster et al. 2012; Hawkins et al. 2014), including different formation times for different halo populations (e.g. Ge et al. 2016). Measurements of stellar ages in the MW bulge suggest that the stellar population is predominantly older than ∼10 Gyr (Barbuy, Chiappini & Gerhard 2018, and references therein).

Cosmological galaxy simulations provide the best theoretical laboratories for understanding the full evolutionary histories of galaxies across cosmic time. It remains unclear if the formation histories of MW/M31-mass galaxies depend on whether they are in isolated environments (with no other nearby companions of similar mass) or in Local Group (LG)-like environments (with a pair of massive galaxies at $\lesssim$1 Mpc separation). Most simulations of MW/M31-mass galaxies, either idealized or cosmological, focus on a *single isolated* galaxy/halo (e.g. AURIGA, NIHAO, ERIS, and Caterpillar), not in an LG-like MW + M31 pair (Guedes et al. 2011; Griffen et al. 2016; Grand et al. 2017; Buck et al. 2020). Exceptions include the ELVIS DM-only (DMO) simulation suite, which includes 24 MW/M31-mass haloes in LG-like pairs and a mass-matched sample of 24 isolated haloes (Garrison-Kimmel et al. 2014), the cosmological baryonic simulations of LG-like pairs from the APOSTLE suite (Sawala et al. 2016), and the simulated LG analogues from the Constrained Local Universe Simulations (CLUES) project (Carlesi et al. 2020). Furthermore, semi-analytic models applied in a cosmological setting provide complementary tools to understand MW-mass formation histories and their environmental dependence. For instance, the semi-analytical code GAlaxy MErger Tree and Evolution (GAMETE, and the similar code GAMESH that accounts for radiative transfer) allows for a detailed modelling for things such as the gas evolution within an MW-mass galaxy, the evolution of the galactic SFR, and the formation/evolution of early Population III (Pop III) stars (Salvadori, Schneider & Ferrara 2007; de Bennassuti et al. 2014; Graziani et al. 2015).

In addition to potential differences in host galaxy properties in LG-like versus isolated environments, it is also imperative to understand potential differences in their satellite populations. While observations of the LG have driven most of our knowledge of dwarf galaxy populations, recent observational campaigns aim to measure satellite populations around (primarily more isolated) MW-mass galaxies such as M94 (Smercina et al. 2018), M101 (Danieli et al. 2017), M81 (Karachentsev & Kudrya 2014), and Centaurus A (Müller et al. 2019). The Satellites Around Galactic Analogs (SAGA) survey[1] also is observing satellite populations around (mostly) isolated MW-mass galaxies down to the luminosity of Leo I ($M_{\rm r} < -12.3$; $M_{\rm star} \approx 5 \times 10^6$ M$_\odot$), with a predicted sample size of 100 galaxies (Geha et al. 2017). Other campaigns instead focus on groups of galaxies out to ∼40 Mpc (e.g. Kourkchi & Tully 2017). In connecting these observations with those of the LG, we must understand: *does environment play a role in the satellite galaxy populations, and thus building blocks, of MW/M31-mass galaxies across cosmic time?*

[1] See the SAGA survey web site: http://sagasurvey.org.

In this work, we use FIRE-2 simulations of 12 MW/M31-mass galaxies to investigate their cosmological hierarchical formation histories. We quantify these galaxies' building blocks across cosmic time and determine when their main progenitors formed/emerged. We investigate the times at which (1) the *stellar* mass growth of the most massive progenitor (MMP) transitions from being dominated by *ex-situ* stars (via mergers) to *in-situ* star formation, and (2) when the most massive galaxy starts to dominate in stellar mass compared to other progenitor galaxies. When a progenitor galaxy satisfies either of these two criteria, we define it to be the 'main' progenitor, which is distinct from the other progenitor galaxies that continue to merge in. There are many definitions of host galaxy 'formation', such as when the main galaxy reaches a fraction of its mass at $z = 0$; here we refer to formation specifically as when a single main progenitor galaxy emerges in its environment, based both on its *in-situ* star formation (Section 3.3) and how its stellar mass compares to its neighbours (Section 3.4). We also emphasize that in our analysis, we focus on the formation of the host galaxy generally, and not specifically on the formation of a given component, such as the thin or thick disc.

Our work, however, is not the first to investigate general properties of the progenitors of MW-mass galaxies and their satellites. Many studies, including those from Dixon et al. (2018), Safarzadeh et al. (2018), Graziani et al. (2017), Magg et al. (2018), and de Bennassuti et al. (2017), have focused on the high-z Universe to study star formation near the epoch of reionization, the metallicity distribution function, identifying ultra-faint dwarf (UFD) galaxy progenitors, and Pop III stars to understand the early MW environment.

The main questions that we address are as follows:

(i) What were the building blocks (progenitor galaxies) of MW/M31-mass galaxies, and how many were there across cosmic time?

(ii) When did the main progenitor of an MW/M31-mass galaxy form/emerge?

(iii) Does the formation of MW/M31-mass galaxies depend on their environment, specifically, comparing isolated hosts to those in LG-like pairs?

2 METHODS

2.1 FIRE-2 simulations of MW- and M31-mass galaxies

We use cosmological zoom-in baryonic simulations of MW/M31-mass galaxies from the FIRE project[2] (Hopkins et al. 2018). We ran these simulations using the Gizmo N-body gravitational plus hydrodynamics code (Hopkins 2015), with the mesh-free finite-mass hydrodynamics method and the FIRE-2 physics model (Hopkins et al. 2018). FIRE-2 includes several radiative cooling and heating processes for gas such as free–free emission, photoionization/recombination, Compton scattering, photoelectric, metal line, molecular, fine structure, dust collisional, and cosmic ray heating across a temperature range of $10–10^{10}$ K. This includes the spatially uniform, redshift-dependent cosmic UV background from Faucher-Giguère et al. (2009), for which H I reionization occurs at $z_{\rm reion} \sim 10$. The simulations self-consistently generate and track 11 elemental abundances (H, He, C, N, O, Ne, Mg, Si, S, Ca, and Fe), including sub-grid diffusion of these abundances in gas via turbulence (Hopkins 2016; Su et al. 2017; Escala et al. 2018).

Stars form from gas that is self-gravitating, Jeans unstable, molecular (following Krumholz & Gnedin 2011), and dense ($n_{\rm H} > 1000$ cm^{-3}). Once a star particle forms, inheriting mass and elemental abundances from its progenitor gas element, it represents a single stellar population, assuming a Kroupa (2001) initial mass function, and it evolves along stellar population models from STARBURST99 v7.0 (Leitherer et al. 1999). FIRE-2 simulations include several different feedback processes, including core-collapse and Ia supernovae, mass-loss from stellar winds, and radiation, including radiation pressure, photoionization, and photoelectric heating.

We generated cosmological zoom-in initial conditions for each simulation at $z \approx 99$, embedded within periodic cosmological boxes of lengths 70.4–172 Mpc using the code MUSIC (Hahn & Abel 2011). We saved 600 snapshots down to $z = 0$, which are spaced every $\approx$25 Myr. All simulations assume flat ΛCDM cosmology with parameters consistent with Planck Collaboration VI (2018). Specifically, the Latte suite (excluding m12w) used $\Omega_{\rm m} = 0.272$, $\Omega_{\rm b} = 0.0455$, $\sigma_8 = 0.807$, $n_{\rm s} = 0.961$, and $h = 0.702$. Thelma and Louise and Romulus and Remus both used the same cosmology as in the original ELVIS DMO suite: $\Omega_{\rm m} = 0.266$, $\Omega_{\rm b} = 0.0449$, $\sigma_8 = 0.801$, $n_{\rm s} = 0.963$, and $h = 0.71$. Finally, Romeo and Juliet and m12w both used $\Omega_{\rm m} = 0.31$, $\Omega_{\rm b} = 0.048$, $\sigma_8 = 0.82$, $n_{\rm s} = 0.97$, and $h = 0.68$.

In this work, we analyse 12 MW/M31-mass galaxies; Table 1 lists their properties. Six galaxies are from the Latte suite of isolated MW/M31-mass galaxies, introduced in Wetzel et al. (2016). We selected these haloes with the following two criteria: (1) $M_{\rm 200m} = (1–2) \times 10^{12}\,{\rm M}_{\odot}$ (e.g. Bland-Hawthorn & Gerhard 2016) and (2) no similar-mass halo within $5 \times R_{\rm 200m}$ (for computational efficiency). Here, $M_{\rm 200m}$ refers to the total mass within a radius, $R_{\rm 200m}$, containing 200 times the mean matter density of the Universe. We chose galaxy m12w with one additional criterion: having an LMC-mass satellite at $z \sim 0$ in the pilot DM-only simulation (see Samuel et al. 2020). The Latte simulations have gas and *initial* star particle masses of 7100 ${\rm M}_{\odot}$, although because of stellar mass-loss, the typical star particle at $z = 0$ is $\sim$5000 ${\rm M}_{\odot}$. DM particles have masses of $3.5 \times 10^4\,{\rm M}_{\odot}$. Gas elements use fully adaptive force softening, equal to their hydrodynamic smoothing, that adapts down to 1 pc. The gravitational softening lengths for star and DM particle are fixed at 4 and 40 pc (Plummer equivalent), comoving at $z > 9$ and physical thereafter.

We also use six galaxies from the 'ELVIS on FIRE' suite of three LG-like MW+M31 pairs (Garrison-Kimmel et al. 2019a, b), which were selected with the following criteria: (1) two neighbouring haloes each with a mass of $M_{\rm 200m} = (1–3) \times 10^{12}\,{\rm M}_{\odot}$, (2) total LG mass of $(2–5) \times 10^{12}\,{\rm M}_{\odot}$, (3) centre separation of 600–1000 kpc at $z = 0$, (4) radial velocities of $v_{\rm rad} < 0\,{\rm km\,s^{-1}}$ at $z = 0$, and (5) no other massive haloes within 2.8 Mpc of either host centre. The ELVIS on FIRE simulations has $\approx 2\times$ better mass resolution than Latte, with initial star/gas particle masses of 3500–4000 ${\rm M}_{\odot}$. Hopkins et al. (2018) examined the effect of mass resolution on the formation histories of both m12i and m12m, finding differences of $\lesssim$10–20 per cent in their star formation histories (SFHs) comparing star particle masses of 7000–56 000 ${\rm M}_{\odot}$. We thus expect that the factor of $\approx 2\times$ resolution difference between the Latte and ELVIS suites should not significantly affect their SFHs.

We simulated these galaxies using the cosmological zoom-in technique (Oñorbe et al. 2014): see Wetzel et al. (2016), Hopkins et al. (2018), and Garrison-Kimmel et al. (2019a) for more details. We emphasize that we selected these haloes solely using the parameters above, with no prior on their formation/merger histories or satellite populations (other than m12w). Furthermore, the numerical implementation that we used to generate these simulations, the Gizmo source code and FIRE-2 physics model, was the same across

[2] See the FIRE project web site: http://fire.northwestern.edu.

Table 1. Properties of the 12 host galaxies in the FIRE-2 simulation suite that we analyse. Column list: name; stellar mass ($M_{\rm star,\,90}$) within $R_{\rm star,\,90}$; disc radius enclosing 90 per cent of the stellar mass within 20 kpc ($R_{\rm star,\,90}$); halo virial mass ($M_{\rm 200m}$); halo virial radius ($R_{\rm 200m}$); redshift when the galaxy reached 50 per cent ($z_{0.5}$) or 10 per cent ($z_{0.1}$) of its stellar mass at $z = 0$; redshift when the cumulative fraction of stars that formed *in situ* exceeded 0.5 when selecting stars at $z = 0$ within host-centric distances of 15 kpc ($z_{\rm in\text{-}situ,\,15}$) and 2 kpc ($z_{\rm in\text{-}situ,\,2}$; redshift when the MMP exceeded a 3:1 stellar mass ratio with respect to the second MMP ($z_{\rm MR,\,15}$); and the paper that introduced each simulation. Hosts with names starting with 'm12' are isolated hosts from the Latte suite, while the rest are in LG-like pairs from the ELVIS on FIRE suite.

Name	$M_{\rm star,90}$ ($10^{10}\,{\rm M}_\odot$)	$R_{\rm star,\,90}$ (kpc)	$M_{\rm 200m}$ ($10^{12}\,{\rm M}_\odot$)	$R_{\rm 200m}$ (kpc)	$z_{0.5}$	$z_{0.1}$	$z_{\rm in\text{-}situ,\,15}$	$z_{\rm in\text{-}situ,\,2}$	$z_{\rm MR,\,15}$	Ref.
m12m	10.0	11.6	1.6	371	0.6	1.5	1.9	2.1	1.5	A
Romulus	8.0	12.9	2.1	406	0.7	1.4	5.3	>6.0	1.7	B
m12b	7.3	9.0	1.4	358	0.6	1.7	2.4	4.2	3.7	C
m12f	6.9	11.8	1.7	380	0.5	2.0	3.7	>6.0	2.9	D
Thelma	6.3	11.2	1.4	358	0.4	1.1	1.7	1.7	4.4	C
Romeo	5.9	12.4	1.3	341	1.0	2.6	>6.0	>6.0	>6.0	C
m12i	5.5	8.5	1.2	336	0.6	1.7	3.1	3.5	1.7	E
m12c	5.1	9.1	1.4	351	0.5	1.3	1.9	5.3	3.1	C
m12w	4.8	7.3	1.1	319	0.4	1.4	2.7	3.4	1.2	F
Remus	4.0	11.0	1.2	339	0.9	2.7	3.7	>6.0	1.2	B
Juliet	3.3	8.1	1.1	321	0.8	2.4	5.3	5.5	4.7	C
Louise	2.3	11.2	1.2	333	0.9	2.5	4.9	5.0	3.5	C

Note. The references for each host are: A: Hopkins et al. (2018), B: Garrison-Kimmel et al. (2019a), C: Garrison-Kimmel et al. (2019b), D: Garrison-Kimmel et al. (2017), E: Wetzel et al. (2016), and F: Samuel et al. (2020).

all simulations. Thus, these 12 hosts should reflect random/typical samplings of MW/M31-mass formation histories within their mass and environmental selection criteria. However, as we show below, LG-like versus isolated host selection does lead to systematically different formation histories.

Both the Latte and ELVIS on FIRE simulation suites form MW/M31-mass galaxies with realistic populations of satellite galaxies, in terms of their stellar masses and velocity dispersions (dynamical masses) (Wetzel et al. 2016; Garrison-Kimmel et al. 2019a), radial distributions (Samuel et al. 2020), and SFHs (Garrison-Kimmel et al. 2019b). The MW/M31-mass host galaxies in the simulations also show a range of morphologies (Garrison-Kimmel et al. 2018; El-Badry et al. 2018a), with properties that broadly agree with the MW and M31, such as the stellar-to-halo mass relation (Hopkins et al. 2018), disc structure and gas mass (Sanderson et al. 2020), age and metallicity gradients (Ma et al. 2017), and stellar haloes (Bonaca et al. 2017; Sanderson et al. 2018). The papers above provide detailed properties for at least some of the hosts. For example, Ma et al. (2017) investigated age and metallicity gradients, as well as the disc structure, of m12i. Sanderson et al. (2018) presented surface densities of both the disc and bulge, and halo stellar masses for *all* simulations used in this work. Sanderson et al. (2020) lists the gas masses, disc scale heights, and SFR (at $z = 0$) for m12f, m12i, and m12m. Several upcoming works will present gas and stellar metallicities (Bellardini et al., in preparation), and the evolution of SFR across redshift (Yu et al., in preparation) for all of these simulated hosts.

2.2 Identifying haloes and galaxies

We use the ROCKSTAR 6D halo finder (Behroozi, Wechsler & Wu 2013a) to identify DM (sub)haloes, using $M_{\rm 200m}$ as our halo definition. We generate a halo catalogue using only DM particles at each of the 600 snapshots and use CONSISTENT-TREES (Behroozi et al. 2013b) to construct merger trees. Given the conservatively large zoom-in volume that we generate for each host, all of the haloes that we examine have zero contamination by low-resolution DM particles.

We briefly summarize the method that we use to assign star particles to haloes in post-processing; see Necib et al. (2019a) and Samuel et al. (2020) for details. Given each (sub)halo's radius and maximum circular velocity, $R_{\rm halo}$ and $V_{\rm circ,max}$, as returned by ROCKSTAR, we identify star particles whose positions lie within 0.8 $R_{\rm halo}$ (out to a maximum distance of 30 kpc) and whose velocities are within 2 $V_{\rm circ,max}$ of the (sub)halo's centre-of-mass velocity. After this, we keep star particles if they meet the following two criteria. First, their positions are within 1.5 $R_{\rm star,\,90}$ (the radius that encloses 90 per cent of the stellar mass) of both the centre-of-mass position of current member star particles and the halo centre. This criterion ensures that the galaxy's centre of mass coincides with the halo's centre of mass. Secondly, their velocities are within 2 $\sigma_{\rm vel,\,star}$, the velocity dispersion of current member star particles, of the centre-of-mass velocity of member star particles. We iterate these two criteria until the stellar mass converges to within 1 per cent. We then keep haloes with at least six star particles, stellar density $> 300\,{\rm M}_\odot\,{\rm kpc}^{-3}$ (at R_{50}, the radius that encloses 50 per cent of the stellar mass), and halo bound mass fraction >40 per cent. Henceforth, when we refer to a galaxy's stellar mass, we mean the mass that we calculate from this process. We checked that none of our results change significantly if we use other ways of measuring stellar mass, such as the mass within $R_{\rm star,\,90}$.

Our software for reading and analysing halo catalogues, including assigning star particles, is available via the HALOANALYSIS package,[3] and our software for reading and analysing particles from Gizmo snapshots is available via the GIZMOANALYSIS package;[4] we first developed and used these packages in Wetzel et al. (2016).

2.3 Selecting progenitor galaxies

In our analysis, we impose two additional criteria to select galaxies of interest. First, we examine only galaxies with a stellar mass of $M_{\rm star} \geq 10^5\,{\rm M}_\odot$, which corresponds to ≥14–29 star particles, depending on simulation resolution. Secondly, we analyse only galaxies that are progenitors of each MW/M31-mass system at $z = 0$, selecting

[3] https://bitbucket.org/awetzel/halo_analysis
[4] https://bitbucket.org/awetzel/gizmo_analysis

stars at various host-centric distances at $z = 0$ to probe the formation histories of different regions of the host galaxy/halo. Specifically, we select progenitor galaxies that contribute star particles to the following spherical distances, d, with respect to the centre of each MW/M31-mass galaxy at $z = 0$:

(i) $d(z = 0) < 300$ kpc (hereon d_{300}), corresponding to the entire host halo system (virial region), including the entire host galaxy, stellar halo, and surviving satellite galaxies;

(ii) $d(z = 0) < 15$ kpc (d_{15}), corresponding to the entire host galaxy (bulge and disc) plus inner stellar halo;

(iii) $d(z = 0) < 2$ kpc (d_2), corresponding to an inner bulge region.

While these represent relatively simple spherical distance selections, we also investigated a 'disc' selection, by selecting stars at $z = 0$ within $R = 4$–15 kpc and $|Z| < 2$ kpc (in cylindrical coordinates), as well as requiring stars to be on co-rotating disc-like circular orbits via Toomre diagram selection. While this reduces the overall amount of accreted stars (as expected), given our method to select progenitor galaxies (see the next paragraph), this selection generally did not lead to significant differences in our results compared to d_{15}.

Having defined the star particles in each region at $z = 0$, to select progenitor galaxies at a given redshift, we compute how much stellar mass a galaxy at a given redshift contributed to these host-centric distances at $z = 0$, relative to the galaxy's total stellar mass at that redshift. We define this as the 'contribution fraction'. To be a progenitor, we require that a galaxy has a contribution fraction greater than 1 per cent, that is at least 1 per cent of its mass (at a given redshift) ends up within the host-centric region. We checked how our metrics for progenitor formation (described in Sections 3.3 and 3.4, and summarized in Section 3.5) changed as we varied this contribution fraction requirement. For d_{300}, our results are not sensitive to it, because all contribution fractions are near 100 per cent, indicating that galaxies that contribute to the host halo contribute essentially all of their stars. For d_2, and to a lesser extent d_{15}, the contribution fractions are more broadly spread throughout 0–100 per cent, because stars from infalling galaxies get deposited across a range of d by $z = 0$. We thus use 1 per cent contribution fraction as a conservative minimum, though we note that increasing this minimum would decrease the number of progenitors to the inner galaxy.

3 RESULTS

To provide visual context to our analysis, Fig. 1 shows synthetic *Hubble Space Telescope u*/*g*/*r* composite stellar images of two of our isolated hosts – m12f (top) and m12m (bottom) – using STARBURST99 to determine the spectral energy distribution (SED) for each star particle (given its age and metallicity) and following the ray-tracing methods in Hopkins et al. (2005, 2018) for an observer 1 Mpc away. These images do not include dust attenuation. Each star particle is represented as a spherical cloud, with size representative of the local density of star particles. These images show stellar luminosity along a given line of sight using a logarithmic colour scale, with visible stellar densities ranging from 10^{-9} to 3×10^{-2} M$_\odot$ pc^{-3}.

Left to right, each panel shows different times throughout the formation of each MW/M31-mass galaxy, including all stars out to 300 kpc (physical) from the MMP. At $z = 0$ (right), the MW/M31-mass host galaxy is clearly dominant, including 16–27 resolved surviving satellite galaxies and an extended stellar halo with stellar streams from disrupted satellites. Some of the visible streams formed via outflows of gas (Yu et al. 2020), while others form via satellite disruption. However, at $z = 5$ (left), the system was composed of a collection of many similar-mass galaxies that eventually merge together. Because many galaxies had similar mass and none of them alone dominated the stellar mass growth, there was no meaningful single 'main' progenitor at this time. The middle panel shows each host when its main progenitor 'formed/emerged', which we define as when the cumulative stellar mass was dominated by *in-situ* formation in a single progenitor (see Section 3.3). We define *in-situ* formation as being star formation that occurs in the MMP; we discuss details of how we calculate the *in-situ fraction* in the beginning of Section 3.3. Similarly, *ex-situ* formation is defined as that which occurs in any other progenitor galaxy; we discuss details about how we determine the *ex-situ fraction* in Section 3.2. Compared to the panels on the left, we see the emergence of a main progenitor galaxy that dominates its local environment in mass by more than 3:1 (see Section 3.4).

3.1 What was the mass growth of the MMP and does it depend on environment?

First, we examine the stellar mass growth history of the MMP of each MW/M31-mass galaxy from $z = 0$ back to $z = 7$. Following the criteria above, we identify the progenitor galaxy with the highest stellar mass at each snapshot (according to our halo catalogue) and label it as the MMP. This is different from using the halo merger tree to track the galaxy back in time, because DM halo and stellar masses grow at different rates, so the most massive halo is not always the most massive galaxy, especially at early times before a main progenitor has emerged. Furthermore, as we argue in Section 3.3, it does not make sense to think about the MMP as the single 'main' progenitor before the 'formation' redshift of each host. Our goal here is to set the stage by providing the relevant mass scale of the MMP across cosmic time while highlighting environmental differences. Also, the results in this section do not depend on the details of host-centric distance selection at $z = 0$, because the MMP contributes significant mass inside all of our distance cuts.

Fig. 2 (top left) shows the stellar mass of the MMP versus redshift (bottom axis) and lookback time (top axis). We show each simulation individually (coloured lines), including six isolated hosts (solid) and six LG-like hosts (dotted). We also show the median across all 12 hosts (thick solid black), and the median for the isolated (thick solid grey) and LG-like (thick dashed grey) hosts. For clarity, we define $M_{\rm star}(z)$ as the stellar mass inside of the MMP galaxy that has formed up to redshift z. At $z = 0$ the host galaxies span a relatively narrow range of $M_{\rm star}(z = 0) = (2.3\text{–}10) \times 10^{10}$ M$_\odot$ (by selection). The shapes of the MMP mass growth histories show broad similarities, with $\log M_{\rm star}$ growing almost linearly with redshift. However, because of scatter in formation history, the $M_{\rm star}$ of MMPs spanned 1–1.5 orders of magnitude at $z \gtrsim 2$ (>10.5 Gyr ago). For example, the MMPs spanned a range of (5.6×10^6)–(7.3×10^7) M$_\odot$ at $z = 7$, near the end of cosmic reionization.

Fig. 2 (top right) shows the same, except we normalize each MMP to the overall median $M_{\rm star}(z)$, which more clearly highlights both scatter in mass growth and systematic differences between LG-like and isolated hosts. In particular, the typical $M_{\rm star}$ of the MMP of an isolated host is similar (slightly higher) than that of an LG-like host at all $z < 1.5$, but prior to this, the MMP of an LG-like host was significantly more massive than that of an isolated host. The biggest difference occurred at $z \sim 4$ (~12.2 Gyr ago), when LG-like hosts were ~6× more massive than isolated hosts.

Fig. 2 (bottom left) shows the *fractional* $M_{\rm star}$ growth of each MMP, that is $M_{\rm star}(z)/M_{\rm star}(z = 0)$. This metric is more fair to compare the formation histories, because it normalizes out the scatter in $M_{\rm star}(z = 0)$. Across all simulations, the MMP reached 10 and

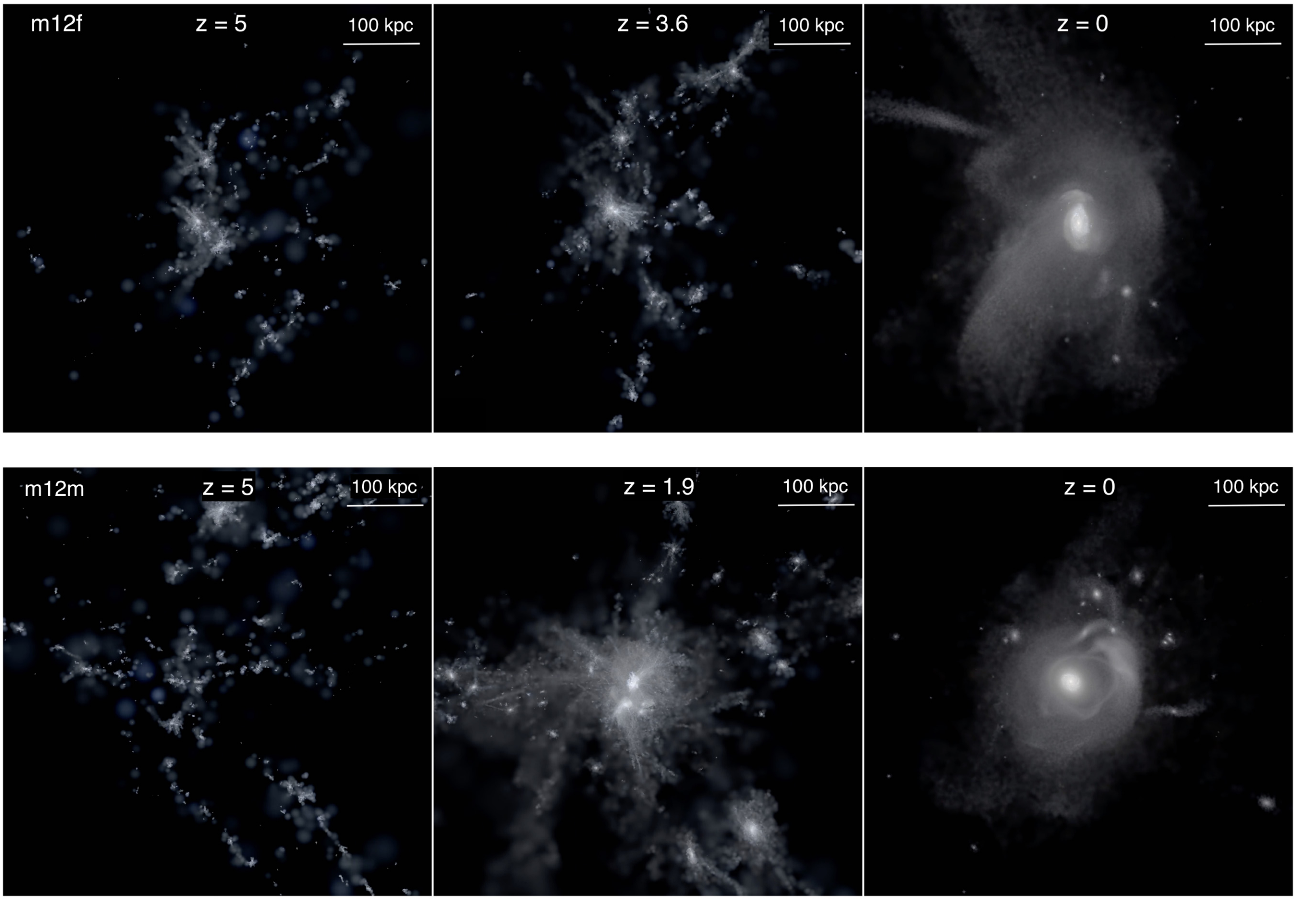

Figure 1. Synthetic *Hubble Space Telescope u/g/r* composite stellar images of all star particles (ignoring dust attenuation) out to a distance of 300 kpc physical (roughly R_{200m} at $z = 0$) around the MMP at each redshift, for two simulations that bracket the main progenitor formation times across our isolated hosts. Each star particle is represented as a spherical cloud, with size representative of the local density of star particles. Intensity is logarithmic with stellar density, the visible regions ranging from 10^{-9} to 3×10^{-2} M$_\odot$ pc^{-3}. Left to right, the panels show images at $z = 5$, $z = z_{\rm form}$ (when the main progenitor 'formed' or 'emerged'), and at $z = 0$. We define main progenitor formation when the majority of stars for d_{15} have formed *in situ* in a single progenitor (see Section 3.3); this is similar to when the stellar mass ratio of the most massive to second MMP exceeds 3:1 (see Section 3.4). The top row shows m12f, our earliest forming isolated host, and the bottom row shows m12m, our latest forming isolated host. *Prior to z_{form}, there was little meaningful sense of a single 'main' progenitor; instead, there was a collection of similar-mass progenitor galaxies.*

50 per cent of its final mass at typically $z = 1.7$ (9.9 Gyr ago) and $z = 0.5$ (5.1 Gyr ago), respectively. Again, the MMP of an isolated host typically formed later, reaching 10 and 50 per cent of its final mass at $z = 1.5$ (9.4 Gyr ago) and $z = 0.5$ (5.1 Gyr ago), while the MMP of an LG-like host typically formed earlier, reaching 10 and 50 per cent of its final mass at $z = 2.4$ (11.0 Gyr ago) and $z = 0.8$ (6.9 Gyr ago).

Finally, Fig. 2 (bottom right) shows the fractional $M_{\rm star}$ growth in the bottom left panel but normalized to the total median (black curve) across all simulations. This metric shows that, by normalizing the curves by their $M_{\rm star}$ at present, the median LG-like host now had higher fractional mass than the median isolated host *at all redshifts*. The biggest difference occurred at $z \sim 4.2$ ($\sim$12.3 Gyr ago), where the medians differed by almost an order of magnitude.

While this offset between LG-like and isolated hosts has some host-to-host scatter, we emphasize that at *all* redshifts, the MMP for four or five of the six LG-like hosts was fractionally more massive than the MMP for *all* of the isolated hosts. This result highlights significant systematic differences in the formation histories of the MMPs in LG-like versus isolated environments. This is important when using cosmological zoom-in simulations such as these to compare with observations of the MW and M31 in the LG or with isolated MW-mass hosts as in, for example, the SAGA survey. We also emphasize that the MMPs of LG-like hosts were systematically more massive even back to $z = 7$, indicating that these environmental effects manifest themselves early, even when the MMPs were only (10^{-4})–(10^{-3}) of their final stellar mass. In Section 3.6, we discuss how this likely follows from the mass growth of the DM host halo.

These trends are consistent with a similar analysis of the archaeological SFHs of these hosts in Garrison-Kimmel et al. (2019b), which calculated SFHs using all stars in the host galaxy at $z = 0$. By selecting stars in the host galaxy at $z = 0$, and using their formation times alone to calculate the SFH of the host galaxy, this ultimately includes stars that originally could have formed in a galaxy other than the MMP. This is different from how we compute the mass growth curves in Fig. 2, where we compute the $M_{\rm star}$ of the MMP at each snapshot. Therefore, this result is not sensitive to the way that one computes the stellar mass growth of the host galaxy.

For comparison, the coloured points/bands in Fig. 2 (bottom left) show observational inferences of $M_{\rm star}(z)$ in MW/M31-mass galaxies. Using a fit for the SFR main sequence to observational data of star-forming galaxies, Leitner (2012, red circles) constructed

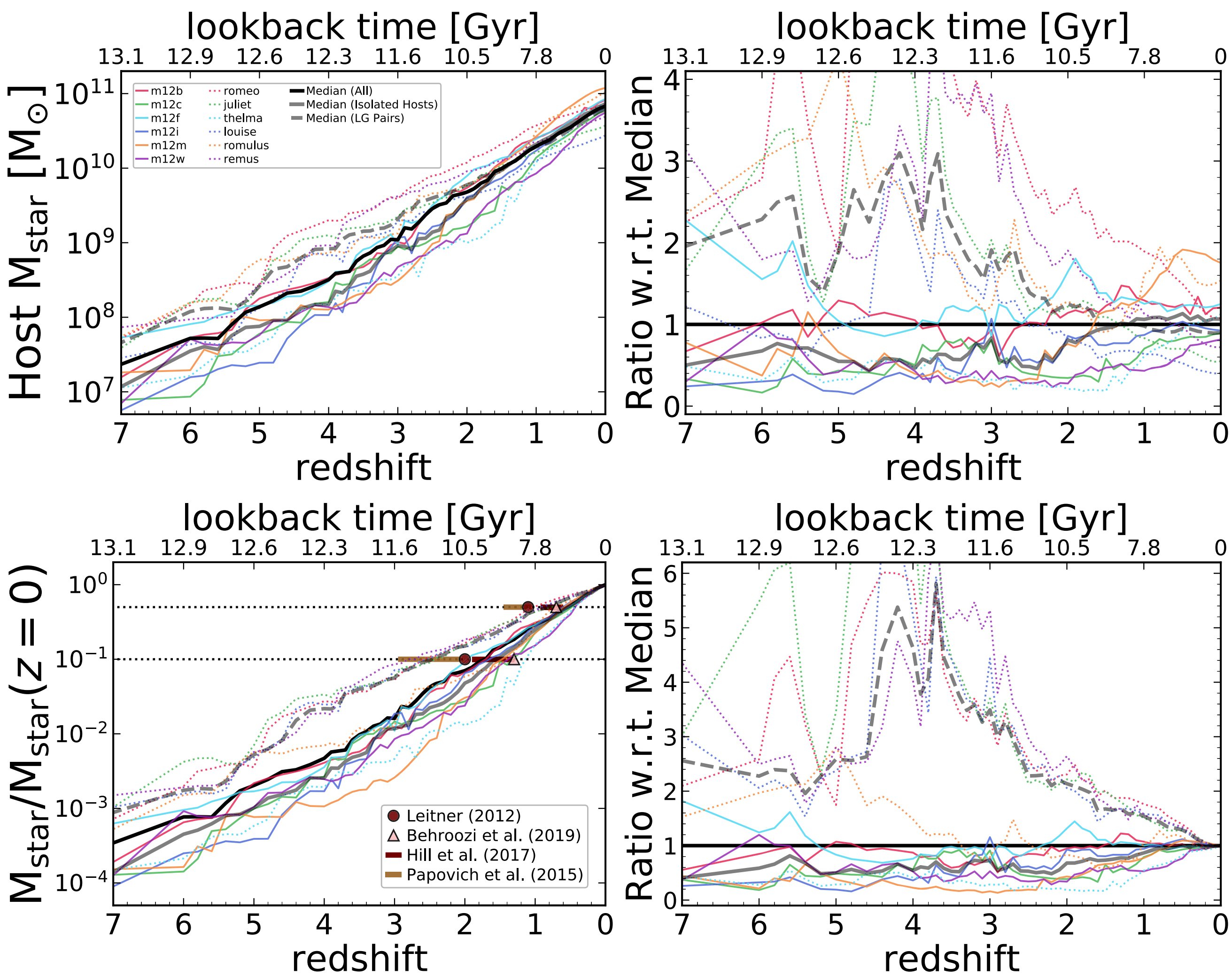

Figure 2. Top left: The stellar mass of the MMP of each MW/M31-mass galaxy as a function of redshift (bottom axis) or lookback time (top axis). Thin coloured lines show each simulation, including the six isolated hosts (solid) and six LG-like hosts (dotted). We also show the median $M_{\rm star}$ across all 12 hosts (thick solid black), and the median for the isolated (thick solid grey) and LG-like (thick dashed grey) hosts. At $z = 0$ the host galaxies span a relatively narrow range of $M_{\rm star}(z = 0) = (2.3–10) \times 10^{10}\,{\rm M}_\odot$ (by selection), but because of scatter in formation history, their MMPs spanned about 1–1.5 orders of magnitude at all $z \gtrsim 4$ (>12.2 Gyr ago), with a range of $(6 \times 10^6)–(7 \times 10^7)\,{\rm M}_\odot$ at $z = 7$, near the end of cosmic reionization. Top Right: Same as left but normalized to the median $M_{\rm star}(z)$ across all simulations. Romeo reached the highest value of ∼6.5 at $z = 4–5$ (12.2–12.6 Gyr ago), while m12i was the lowest at ∼0.15. *The MMPs of LG-like paired hosts had significantly higher mass on average, by up to a factor of 6, at all* $z \gtrsim 2$. Bottom left: Same as top left but showing *fractional* mass growth, with each MMP normalized by its $M_{\rm star}(z = 0)$. The dotted horizontal lines indicate 10 and 50 per cent of final mass. Considering the overall median, the MMP reached 10 per cent of its final mass by $z \sim 1.7$ (9.9 Gyr ago), while for isolated hosts it was $z \sim 1.5$ (9.4 Gyr ago) and for LG-like pairs it was $z \sim 2.4$ (11.0 Gyr ago). The MMP reached 50 per cent of its final mass by $z \sim 0.5$ (5.1 Gyr ago) across all hosts (and isolated host), and while this occurred at $z \sim 0.8$ (6.9 Gyr ago) for LG-like hosts. We also plot observational inferences for galaxies that span our mass range at $z = 0$ (see the text). Bottom right: Same as bottom left, but normalized to the total median: $[M_{\rm star}(z)/M_{\rm star}(z = 0)]\,/\,[M_{\rm star}(z)/M_{\rm star}(z = 0)]_{\rm med}$. Here, the enhancement for LG-like hosts is even most dramatic, *persisting at all redshifts and being almost 10× that of isolated hosts at* $z \sim 4.2$ (12.3 Gyr ago). This highlights the importance of environment in MW/M31-mass galaxy formation, especially at early times.

mass growth histories, finding that galaxies of $M_{\rm star}(z = 0) \sim 10^{11}$ reached 10 per cent of their final mass at $z \approx 2$ (10.4 Gyr ago), and 50 per cent of their final mass at $z \sim 1.1$ (8.2 Gyr ago). These values are broadly consistent with our LG-like hosts, though they are earlier than our typical isolated host, but our hosts have somewhat lower $M_{\rm star}(z = 0)$ than that in Leitner (2012), so this may not be surprising. In another study, Papovich et al. (2015) used abundance matching to find progenitors of MW/M31-mass galaxies, and calculated their stellar mass evolution, taking into account mass-loss from stellar evolution. Galaxies with $M_{\rm star}(z = 0) = 5 \times 10^{10}$ and $10^{11}\,{\rm M}_\odot$ (akin to the MW and M31) tend to reach 10 per cent of their final mass around $z \sim 2–3$ and 50 per cent around $z \sim 1–1.5$, respectively. We represent these redshift ranges via the light brown bands in the bottom left panel and note that these results are consistent with the curves for our LG-like hosts. More recently, Hill et al. (2017) also used abundance matching of stellar mass functions at various redshifts to track MW/M31-mass growth histories (e.g. van Dokkum et al. 2013). Hill et al. (2017) found that 10 per cent mass occurred at $z \sim 1.3–1.9$ (8.9–10.2 Gyr ago) for $10^{10.5-11}\,{\rm M}_\odot$ galaxies, and 50 per cent mass occurred at $z \sim 0.6–0.9$ (5.8–7.4 Gyr ago). We show this range (which brackets our simulation sample) via two dark red bands in Fig. 2, which also broadly agree with our simulation suite, though we note that the typical 50 per cent mass in our simulations occurs slightly later than all of these observational estimates. Finally, Behroozi et al. (2019) (pink triangles) used the Bolshoi–Planck DM-only (DMO) simulation, combined with observed properties of galaxies such as stellar mass functions and SFRs to determine the SFHs of galaxies with $M_{200m} = 10^{12}\,M_{\odot}$ (similar to our sample). They found that these galaxies reached 10 and 50 per cent of their final M_{star} around $z \approx 1.3$ and 0.7 ($\approx$8.9 and $\approx$6.4 Gyr ago, respectively), which are consistent with the typical values in our simulations.

3.2 What were the building blocks of the galaxy?

We next investigate the distribution of 'building blocks' of our MW/M31-mass host galaxies by analysing the cumulative stellar mass function (the number of galaxies above an M_{star} threshold) of all progenitor galaxies (*including* the MMP) across time. We select progenitors that contribute to each of our host-centric distance cuts at $z = 0$. In Fig. 3, the left-hand panels show the median number of progenitor galaxies for the isolated (solid lines) and LG-like (dashed lines) hosts versus redshift using M_{star} thresholds. The shaded regions show 68 per cent scatters across our total sample. The panels on the right show the median number of progenitors across the total sample versus M_{star} at given redshifts (we do not show isolated and LG-like hosts separately here).

Fig. 3 highlights several interesting trends. For the lowest mass progenitors that we resolve ($M_{star} > 10^5\,M_{\odot}$), the number of progenitor galaxies peaked at $z \sim 4$–5 (12.2–12.6 Gyr ago) for all host distance selections. For d_{300}, the number of progenitors peaked at $\sim$85–100, while for d_{15} it peaked at $\sim$55, and for d_2 it peaked at $\sim$20. Given hierarchical structure formation, there were fewer higher mass progenitors, and their numbers peaked at progressively later times. For example, for d_{300}, the number of progenitors with $M_{star} > 10^7\,M_{\odot}$ peaked at $\sim$10 at $z \sim 2.5$. We see similar trends for 15 and 2 kpc distance cuts, though the progenitor peaks shift to larger redshifts, indicating that the increasingly central regions of the MMP formed earlier. For our highest stellar mass cut, $M_{star} > 10^9\,M_{\odot}$, the hosts typically have only one progenitor (the MMP itself). However, both the MW (with the LMC) and M31 (with M32 and M33) have 1–2 satellites above this mass today. While none of our hosts possess such massive satellites at $z = 0$, half of our hosts (6 of 12) have had at least one satellite with $M_{star} > 10^9\,M_{\odot}$ since $z = 0.7$ (Chapman et al., in preparation), but these massive satellites merge into the host galaxy quickly because of efficient dynamical friction, resulting in the instantaneous median number being 0 across all simulations.

The top right panel also shows the number of progenitors at each redshift normalized to the surviving satellites within 300 kpc at $z = 0$. Compared to the present satellite galaxy population, there were nearly $\sim$5 times as many dwarf galaxies that formed each entire MW/M31-mass system, with their numbers peaking at $z \sim 4$ (12.2 Gyr ago). Most of these low-mass progenitors have become disrupted into the main galaxy today. This has implications for galactic archaeology and the 'ear-far' connection, specifically for any attempt to use present-day nearby dwarf galaxies to make inferences about the high-redshift universe (see Section 4.2). Note that the bottom right two panels show just one galaxy (the host galaxy) at $z \sim 0$, because typically these hosts have no resolved satellites inside of 15 kpc (Samuel et al. 2020). For d_{15}, typically 10 progenitor galaxies have contributed to its formation since $z = 1$ (7.8 Gyr ago), while typically only 1–2 progenitors other than the MMP have contributed to the bulge region at $z \lesssim 2$.

We note that for all host distance cuts, the mass function of progenitors was increasingly steeper at higher redshifts, which is consistent in both observational and simulation results of the general galaxy population (e.g. Graus et al. 2016; Song et al. 2016; Ma et al. 2018; see Section 4.2 for more discussion).

Finally, the satellite populations of isolated and LG-like hosts do not differ substantially across time, as seen in the left-hand panels of Fig. 3. For mass bins with $M_{star} \geq 10^7\,M_{\odot}$, LG-like hosts initially had more progenitors, reflective of their earlier formation histories, but they are soon outnumbered compared to the isolated hosts. These differences, however, are small and the right-hand panels show the same behaviour, so we present only the total median in those cases.

Fig. 3 shows that the lowest mass progenitors dominated by number. However, this does not mean that the lowest mass progenitors dominated the *ex-situ* mass of the host (that is, the stellar mass that formed in progenitor galaxies other than the MMP). To quantify this, at each redshift we take the population of progenitors in Fig. 3 (right-hand panels), excluding the MMP, and we weight each progenitor by their contribution fractions. This gives us the stellar mass in these galaxies, which formed before this redshift, that eventually gets deposited into the host. We then divide this quantity by the total stellar mass in the host at $z = 0$ (for the different distance selections d_{300}, d_{15}, and d_2), to obtain the *ex-situ* fraction, $f_{ex\text{-}situ}(M_{star}, > z)$; we show this in Fig. 4. This represents the fraction of stellar mass within the distance selections of the host at $z = 0$, which is above a given age and formed in progenitors of a given M_{star} (other than the MMP). Note that this does not equal the total fraction of M_{star} formed *ex situ at all redshifts* within each host at $z = 0$ (see Fig. 5 for that). Instead, we analyse the *ex-situ* fraction for stars formed before a given redshift, to highlight trends if one selects stars of minimum age in the MW or M31 today.

Fig. 4 shows $f_{ex\text{-}situ}(M_{star}, > z)$ versus progenitor M_{star}. The curves in the left-hand panels show the fraction of stellar mass (which formed before a given redshift) that ends up within the three host-centric distances at $z = 0$, which formed inside progenitors other than the MMP, as a function of progenitor stellar mass. The right-hand panels show the cumulative *ex-situ* fraction that formed in progenitors below a given stellar mass. The shaded regions in all the panels show the 68 per cent scatter across the simulations. In some cases on the left-hand panels, given our finite sample of simulations, the lower scatter goes to zero, that is in some simulations no progenitors at that mass contributed any stars. For visual clarity, we set those values for the lower scatter equal to the median.

Because the slope of the (differential) progenitor mass function, $dN/d\log M$, is shallower than unity, weighting progenitors by their M_{star} means that more massive progenitors (other than the MMP) dominated the *ex-situ* mass, while the contributed M_{star} from the lowest mass galaxy progenitors was comparatively negligible. Also, as a result of hierarchical structure formation, at later times increasingly more massive progenitors dominated the *ex-situ* mass. For stellar populations of *all* ages at $z = 0$, the *ex-situ* mass is dominated by the MMPs, but that mass scale decreases with increasing age.

All of our host-centric distance cuts at $z = 0$ show the same trends above. The primary difference is that regions closer to the centre of the host at $z = 0$ have lower *ex-situ* fractions (normalizations) at all progenitor masses. In other words, the *ex-situ* contribution becomes increasingly negligible towards the central regions of the host galaxy.

While we do not show it separately in Fig. 4 (see instead Fig. 5), we find that isolated hosts had larger *ex-situ* fractions on average than

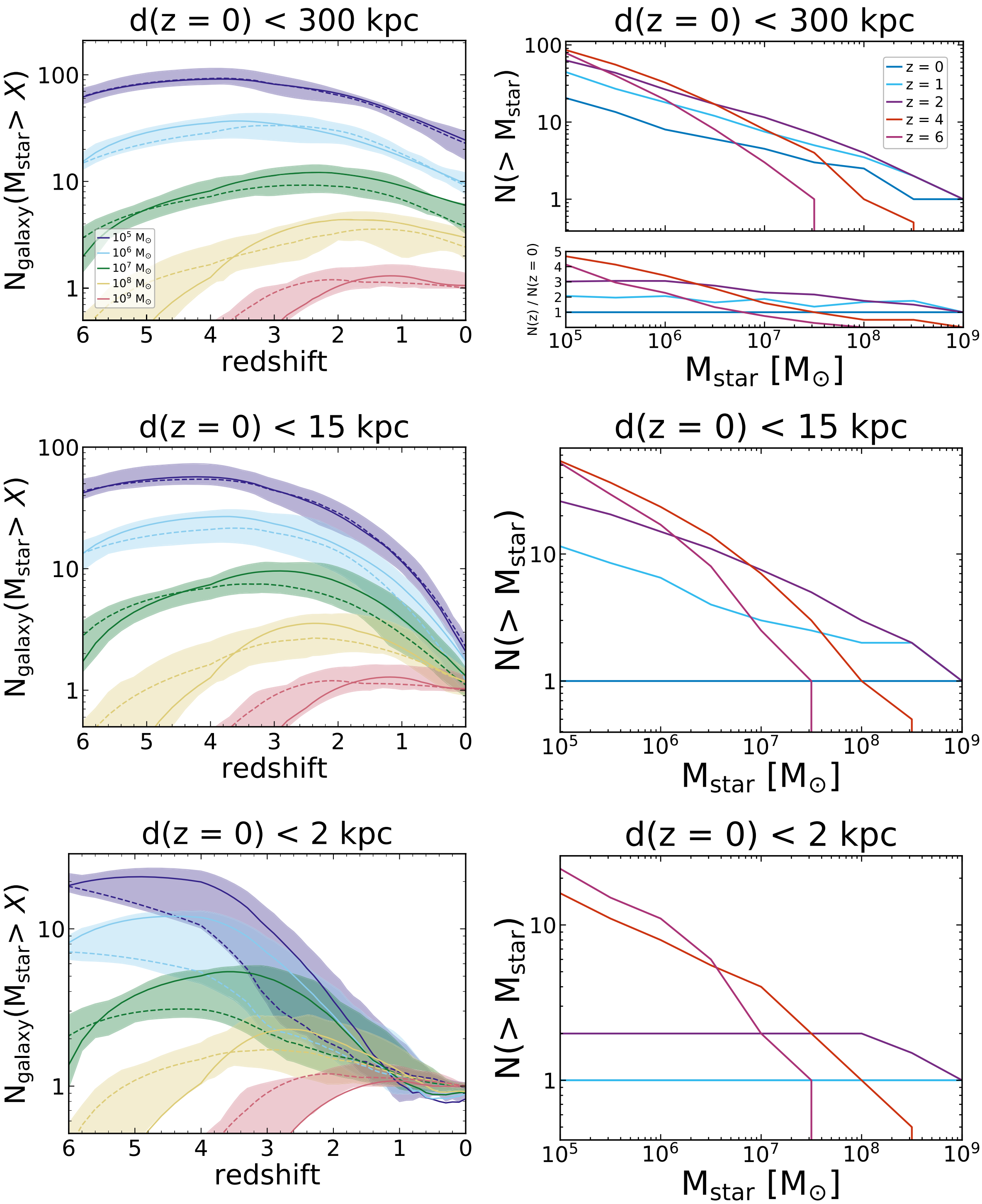

Figure 3. Left: The number of progenitor galaxies above a given stellar mass versus redshift. Progenitor galaxies are those whose stars end up within the given host-centric distances at $z = 0$: the entire host halo (top), the host galaxy + inner stellar halo (middle), and the inner bulge region (bottom). The lines show the median for our 6 isolated (solid) and 6 LG-like (dashed) hosts, while the shaded regions show the 68 per cent scatter across all 12 hosts. Both LG-like and isolated hosts show the same general trends, though the progenitor population of isolated hosts peaks slightly later. Right: Cumulative number of progenitor galaxies versus stellar mass at different redshifts, for the median across all 12 hosts. For d_{300} (top), the lower panel shows the number at each redshift normalized to the number at $z = 0$, that is the population of progenitors relative to surviving satellites at $z = 0$. Note that the progenitor mass function becomes increasingly steeper at higher redshifts (for more discussion, see Section 4.2). Higher mass progenitors contributed preferentially at later times. For $M_{\rm star} > 10^5\,{\rm M}_{\odot}$, ∼85–100 progenitor galaxies contributed to the formation of an MW/M31-mass system out to its halo virial radius, ∼55 contributed to the galaxy within 15 kpc, and ∼20 contributed to the inner bulge region within 2 kpc, with the number of progenitors peaking at $z \sim 4$. Thus, the current satellite population at $M_{\rm star} > 10^5\,{\rm M}_{\odot}$ represents only ∼1/5 of the population that formed each system.

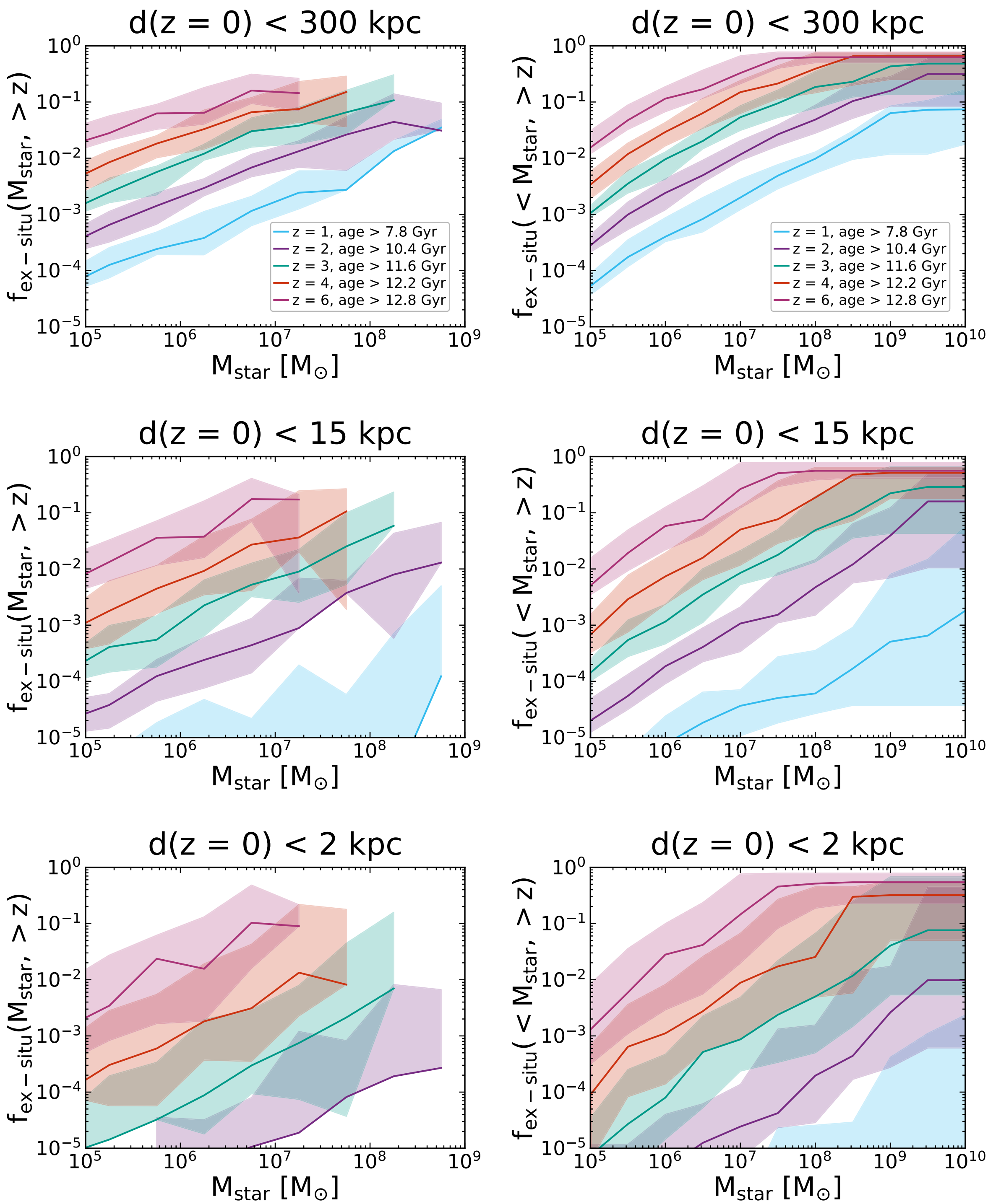

Figure 4. For all stars that end up within the given host-centric distances at $z = 0$ (top to bottom) and that formed before the given redshifts (different coloured lines), the panels show the fraction that formed *ex situ* (in progenitors other than the MMP) as a function of progenitor stellar mass. The left-hand panels show the (differential) fraction within the $M_{\rm star}$ bin, while the right-hand panels show the cumulative fraction less than $M_{\rm star}$. Lines show total median while shaded regions show 68 per cent scatter across all 12 hosts (see the text for discussion of the differences between isolated and LG-like hosts). Because of our sample size, the lower scatter for some mass bins is 0: In these cases, we set the lower scatter equal to the median for visual clarity. For all host-centric distances, the *ex-situ* fraction increases monotonically with increasing redshift and with increasing progenitor mass, so more massive progenitors *always* dominate the *ex-situ* mass.

the LG-like hosts. Specifically, the *ex-situ* fractions for isolated hosts were primarily at the upper end of the 68 per cent scatter region, and LG-like hosts were primarily near the lower end. Thus, *ex-situ* growth is more important for isolated hosts, but any differences converge by $z \sim 1$.

3.3 When did *in-situ* star formation dominate the mass growth?

Having explored the *ex-situ* fraction as a function of progenitor mass, we next examine the total *in-situ* fraction for each host. We aim to understand the transition from (1) an early period when most

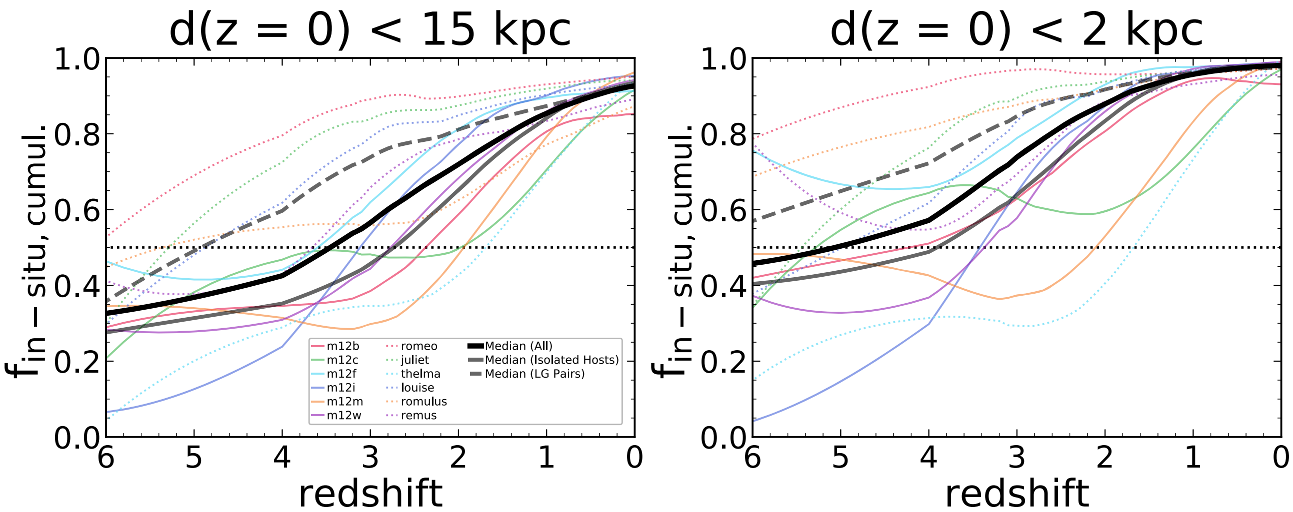

Figure 5. The cumulative *in-situ* fraction, defined as the fraction of all stars that formed prior to a given redshift that formed within the MMP. Thin coloured lines show each simulation, including six isolated hosts (solid) and six LG-like hosts (dotted). We also show the median across all simulations (thick black line), across isolated hosts (solid grey line), and across LG-like hosts (dashed grey line). The horizontal black dotted line at 0.5 shows our definition for progenitor 'formation', above which the host galaxy has transitioned to having formed the majority of its stars *in situ*. Selecting all stars within 15 kpc at $z = 0$, the median progenitor formation across all 12 hosts occurred at $z = 3.5$ (12.0 Gyr ago). For stars in the inner/bulge region, d_2, the main progenitor emerged earlier, at $z = 5.2$ (12.6 Gyr ago). Reflective of Fig. 2, for d_{15}, progenitor formation occurred earlier for LG-like hosts ($z = 4.9$, 12.5 Gyr ago) than isolated hosts ($z = 2.7$, 11.3 Gyr ago). For d_2, isolated host progenitors formed at $z = 3.9$ (12.2 Gyr ago), while LG-like hosts were never below 0.5, that is the majority of stars at all ages in their bulge region today formed *in situ* in the MMP. *Thus, main progenitors of LG-like paired hosts formed/emerged significantly earlier.*.

stars formed *ex situ* across several progenitors that (eventually) merge together, to (2) a later period when a single main progenitor dominated the stellar mass growth via *in-situ* star formation. Thus, we define '*in-situ*' star formation as that occurring in the MMP, and we define main progenitor 'formation' (or 'emergence') as the transition from (1) to (2). This is different from other definitions of progenitor 'formation', such as when the galaxy formed a certain percentage of its current $M_{\rm star}$ (see Section 3.1). Our goal is instead to quantify when a single main progenitor dominated the stellar mass assembly. To calculate the fraction of *in-situ* star formation, we select stars within the host-centric distance selections at $z = 0$ that are older than a given redshift. Of these, we then select the stars that formed inside of the MMP, and divide this stellar mass by the total stellar mass at $z = 0$ that is older than this redshift. Finally, we cumulatively sum these fractions to get the $f_{\rm in\text{-}situ,cumul}$, shown in Fig. 5.

Fig. 5 shows this cumulative *in-situ* fraction as a function of redshift for the d_{15} and d_2 distance selections. We show each simulation as a thin coloured line (solid for isolated hosts, dotted for LG-like hosts), along with medians for the total, isolated, and LG-like hosts. The horizontal dotted line shows a cumulative *in-situ* fraction of 0.5, which we use to define the formation of a single 'main' progenitor.

Across all 12 hosts, the median formation of the whole galaxy (left-hand panel) occurred at $z \sim 3.5$ (12.0 Gyr ago), and at this redshift, the MMP was ∼1 per cent of its present $M_{\rm star}$ (see the bottom left panel in Fig. 2) and the MMP halo was ∼10 per cent of its present $M_{\rm 200m}$ (Fig. 8). Formation in LG-like and isolated hosts occurred around $z = 4.9$ (12.5 Gyr ago) and $z = 2.7$ (11.3 Gyr ago), respectively. However, both host types converged to similar *in-situ* fractions by $z \lesssim 1$ (7.8 Gyr ago), so these environmental differences were important only in early formation. The median cumulative *in-situ* fraction at $z = 0$ is ∼93 per cent, which is consistent with previous results in Anglés-Alcázar et al. (2017), who analysed the FIRE-1 simulations (including a version of m12i) and found that *in-situ* star formation dominates ≥95 per cent of the stellar mass growth at MW masses. The NIHAO simulations also show similar *in-situ* fractions (Buck et al. 2020).

Consistent with (radial) inside-out formation, the inner bulge region of the host (right-hand panel) established itself in a single main progenitor earlier than the overall galaxy, with median formation at $z \sim 5.2$ (12.6 Gyr ago). Interestingly, the median for LG-like hosts never extended below 0.5, at least back to $z = 6$ (12.8 Gyr ago), meaning that these stars formed in a single main progenitor *at all redshifts that we probe*. By contrast, bulge stars in isolated hosts formed in a single main progenitor only at $z \lesssim 3.9$ (12.2 Gyr ago).

While we have presented the *cumulative in-situ* fraction, considering all stars that formed to a given redshift, we also examined the *instantaneous in-situ* fraction, using stars that formed within a narrow bin of redshift (not shown). While this is a more time variable/stochastic metric, we found similar trends overall. The key difference is that, because the *in-situ* fraction rises with decreasing redshift, the cumulative value, being an integral quantity, is smaller than the instantaneous value at a given redshift. Thus, a galaxy transitions above 0.5 at a smaller redshift (typically $\Delta z \sim 0.25$, $\Delta t \sim 0.12$ Gyr) when considering the cumulative *in-situ* fraction. Both fractions show the same dependence on host-centric distance selection and the same trend that LG-like hosts formed earlier. We also note that the *in-situ* fraction for the host 'disc' selection, mentioned in Section 2.3, is similar to d_{15}, with comparable formation times.

Finally, while we discuss median trends above, we emphasize *significant* host-to-host scatter in Fig. 5. For example, for the d_{15} selection, Romeo never had an *in-situ* fraction below 0.5 back to $z = 6$ (12.8 Gyr ago), while Thelma become dominated by *in-situ* mass growth only at $z < 1.7$ (9.9 Gyr ago). We also note that the *in-situ* fractions for some hosts can temporarily decline with time. For instance, in m12c the *in-situ* fraction decreased from $z \sim 4$ to

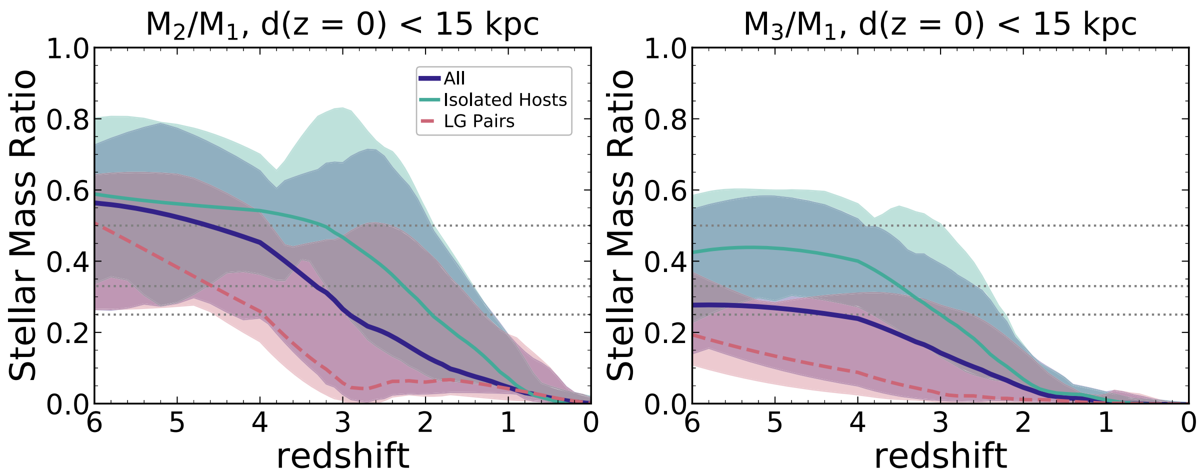

Figure 6. For all progenitor galaxies that contribute stars to host-centric d_{15}, the ratio of the stellar mass of the second (M_2, left) or third (M_3, right) most massive galaxy to that of the MMP (M_1) versus redshift. We show the (smoothed) median across all 12 hosts (solid purple), isolated hosts (solid green), and LG-like hosts (dashed salmon), with the 68 per cent scatter across all hosts in the shaded regions. The horizontal dotted lines show 1:2, 1:3, and 1:4 mass ratios for reference. When each system crosses below these values, the MMP (M_1) increasingly becomes the dominant galaxy across all progenitors. Across all 12 hosts, this transition occurred at $z = 4.6$ (12.5 Gyr ago), $z = 3.3$ (11.8 Gyr ago), and $z = 2.9$ (11.5 Gyr ago) for 1:2, 1:3, and 1:4 ratios in M_2/M_1. M_3 is rarely within a factor of 2 of M_1, and M_3/M_1 drops below 1:4 at $z = 4.2$ (12.3 Gyr ago). Again, the MMP of LG-like hosts becomes dominant earlier than for isolated hosts: M_2/M_1 for LG-like hosts crossed below 1:2, 1:3, and 1:4 at $z = 6$ (12.8 Gyr ago), $z = 4.6$ (12.5 Gyr ago), and $z = 3.9$ (12.2 Gyr ago), while for isolated hosts these transitions occurred at $z = 3.3$ (11.8 Gyr ago), $z = 2.3$ (10.9 Gyr ago), and $z = 1.9$ (10.2 Gyr ago).

2 (12.2–10.4 Gyr ago), which indicates enhanced star formation in progenitors other than the MMP.

Overall, the general trends for both host-centric distance selections are: (1) LG-like hosts formed earlier than isolated hosts, (2) the median and scatter tend to converge at $z \lesssim 1$ (7.8 Gyr ago), and (3) no single progenitor forms later than $z \sim 1.7$ (9.9 Gyr ago).

3.4 When did a dominant-mass progenitor emerge?

Having examined the *in-situ* fraction of star formation, we also examine a second metric of main progenitor 'formation': when the (instantaneous) stellar mass of the single MMP galaxy dominated that of any other progenitor. Fig. 6 shows the ratios of the second and third MMPs relative to the MMP, M_2/M_1 and M_3/M_1 (left- and right-hand panels respectively), as a function of redshift, for progenitors that contribute stars to d_{15}. We show the median across all 12 hosts (solid purple), 6 isolated hosts (solid green), and 6 LG-like hosts (dashed salmon), as well as their respective 68 per cent scatters via the shaded regions. Fig. 6 also shows stellar mass ratios of 1:2, 1:3, and 1:4 via horizontal dotted black lines.

We find the same qualitative trends in both the panels, so we focus primarily on M_2/M_1. However, we note that the median M_3/M_1 ratios were rarely above 1:4 across the total sample, and transitioned below this near $z \sim 4.2$ (12.3 Gyr ago). The (higher) median for the isolated hosts never reached 1:2, and it transitioned below 1:4 later, around $z \sim 3$ (11.6 Gyr ago).

Focusing on the M_2/M_1 ratio (left), we again find that LG-like hosts formed earlier than isolated hosts. Using 1:3 as a fiducial mass ratio, the redshifts where the medians crossed below 1:3 were $z = 4.6$ (12.5 Gyr ago) and 2.3 (10.9 Gyr ago) for the LG-like and isolated hosts, respectively, which is consistent with values in the previous section for d_{15}. If we examine all simulations, this transition occurred between the two at $z = 3.3$ (11.8 Gyr ago). Again, the MMP was $\sim$1 per cent of its present $M_{\rm star}$ at these redshifts, meaning that *the main progenitor formed/emerged as the dominant galaxy well before it formed most of its current mass*. For context, the present ratio of $M_{\rm star}$ between the LMC and the MW is about 1:30 ($\sim$0.033) and for M33 and M31 it is roughly 1:20, or $\sim$0.047 (see compilation in Garrison-Kimmel et al. 2019a).

While we focus on the median trends, we again emphasize the significant scatter in formation histories. We also checked our results using selection of both $d(z = 0) < 300$ and < 2 kpc and saw little change, because the MMP contributes stars throughout the host galaxy at $z = 0$.

3.5 When did the main progenitor form?

Here, we present the redshifts corresponding to our definitions of progenitor formation regarding the two metrics in Sections 3.3 and 3.4: the cumulative *in-situ* star formation fraction and the M_2/M_1 (instantaneous) $M_{\rm star}$ ratio. For the *in-situ* fractions, we use 0.5 as our fiducial threshold to determine when the progenitor formed. Regarding the mass ratio, we choose 1:3 to define formation; this metric does not depend on host-centric distance selection. Fig. 7 shows the total median, as well as the medians of isolated and LG-like hosts separately, with the 68 and 95 per cent scatter in the dark and light vertical bars, respectively.

Considering main progenitor formation based on *in-situ* star formation for d_{15}, the median formation for all 12 hosts, isolated hosts, and LG-like hosts occurred at $z = 3.5$ (12.0 Gyr ago), 2.7 (11.3 Gyr ago), and 4.9 (12.5 Gyr ago), respectively, but the scatters cover a wide range of $z \sim 1.7 - 6$ (9.9–12.8 Gyr ago). For d_2, because the median for LG-like hosts never extended below 0.5 at $z < 6$, we set their formation redshift to be $z = 6$ as a lower limit, making the total, isolated, and LG-like host medians $z = 5.1$ (12.6 Gyr ago), 3.9 (12.2 Gyr ago), and 6 (12.8 Gyr ago), with similar redshift scatter. LG-like hosts had earlier formation times, and we see the same trend of earlier formation for smaller host-centric distance cuts.

If we instead examine main progenitor formation based on instantaneous stellar mass ratio, it reached 1:3 at $z = 3.3$ (11.8 Gyr ago), 2.3 (10.9 Gyr ago), and 4.6 (12.5 Gyr ago) for the total sample,

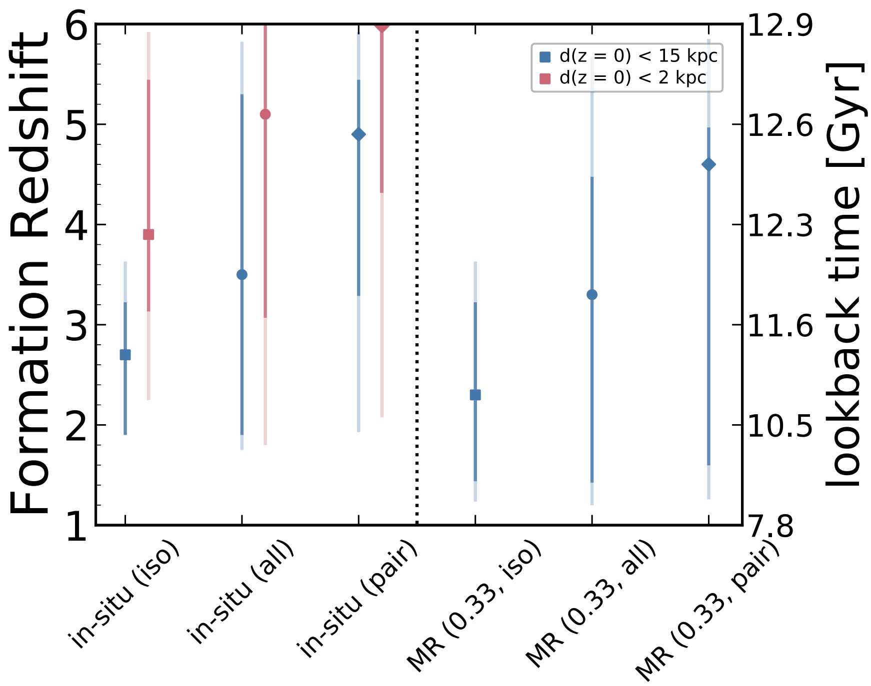

Figure 7. Summary of the 'formation' redshifts (left axis) or lookback times (right axis) of the main progenitors of our simulated MW/M31-mass galaxies. The left half shows formation defined when the cumulative fraction of stars that formed *in situ* exceeds 0.5 (see Section 3.3), selecting stars at two host-centric distances at $z = 0$, corresponding to the galaxy + inner stellar halo, d_{15} (blue points), and the inner bulge region, d_2 (red points). The right half shows formation defined when the MMP exceeds a 3:1 stellar mass ratio with respect to the second MMP (see Section 3.4). Points show the median across the sample and vertical bars show the 68 per cent (darker) and 95 per cent (lighter) scatters, using all 12 hosts (circles), only 6 isolated hosts (squares), and only 6 LG-like hosts (diamonds). For the LG-like hosts at d_2, we show the *in-situ* formation redshift at $z = 6$ (12.8 Gyr ago) as a lower limit. Considering the entire host galaxy, the main progenitor formation times are similar for *in-situ* and 3:1 mass-ratio metrics, being $z \sim 3.4$ (11.9 Gyr ago) for the full sample, though significantly later at $z \sim 2.5$ (11.1 Gyr ago) for isolated hosts and earlier at $z \sim 4.7$ (12.5 Gyr ago) for the LG-like paired hosts, with *significant* scatter across different hosts.

isolated hosts, and LG-like hosts, respectively, with scatter of $z \sim$ 1.2–5.8 (8.6–12.8 Gyr ago). Again, LG-like hosts formed earlier, and we find similar median formation times compared with *in situ*-based formation.

3.6 Does the mass growth of the DM halo depend on environment?

Finally, we seek to understand more deeply why the MMP of an LG-like host experiences more rapid stellar mass growth (Fig. 2) and earlier 'formation' of a main progenitor (Fig. 5) than isolated hosts. Specifically, we investigate whether the mass growth of the DM halo reflects these trends as well. We proceed as with Fig. 2, but instead we measure the DM halo mass of the MMP galaxy. For most progenitors, the highest mass galaxy resides in the highest mass halo. However, because of scatter in stellar versus halo mass growth, especially at early times when there was no clear main progenitor, the MMP galaxy might not reside in the MMP halo. In these cases, we select the halo with the highest DM halo mass as the MMP, but we find nearly identical results if instead we show the DM halo mass of the most massive galaxy.

As Fig. 8 shows, we find qualitatively similar results for halo mass growth as for stellar mass growth: LG-like hosts grow in mass more rapidly than isolated hosts. Specifically, across all 12 hosts, the MMP halo reached 10 per cent of its final mass by $z \sim 3.3$ (11.8 Gyr ago), but isolated hosts reached this later at $z \sim 3$ (11.6 Gyr ago) and LG-like hosts reached it earlier at $z \sim 4$ (12.2 Gyr ago), with $\Delta z \sim 1$ and $\Delta t \sim 0.6$ Gyr. At later times ($z \lesssim 2$), we find some enhanced growth for LG-like hosts, but the mass growth histories are more similar, so this environmental effect is weaker for later term halo growth. These median redshifts are all *earlier* than those for stellar mass in Fig. 2, given that central gravitational potential of a DM halo establishes itself earlier than galaxy that it hosts.

We thus conclude that these differences in halo mass growth likely cause (at least to first order) the differences in stellar mass growth and satellite populations, especially because these environmental differences persist back to the initial collapse of theses haloes at $z \gtrsim 7$. This is perhaps not surprising, given that haloes in LG-like environments formed in denser regions that should collapse earlier than isolated haloes (Gallart et al. 2015).

Using a larger sample of 24 paired and 24 isolated host haloes in the ELVIS DMO suite of simulations, Garrison-Kimmel et al. (2014) did not find major differences in the median formation times of LG-like haloes compared with isolated haloes. Similarly, a study by Forero-Romero et al. (2011) using DMO simulations from both the CLUES project and Bolshoi (Riebe et al. 2013) did not see differences in the formation times of isolated versus LG-like hosts. However, both of these works measured halo 'formation' based on the redshift when a halo formed 50 per cent of its final mass at $z = 0$. Garrison-Kimmel et al. (2014) found that both isolated and LG-like hosts had $z_{\rm form} \sim 1.1$, and we find nearly identical results for our baryonic simulations. The key difference in Fig. 8 is the *early* formation history of the DM halo, which appears to affect the stellar mass growth to even lower redshifts, as evidenced in Fig. 2, where stellar mass growth histories of LG-like versus isolated hosts diverge at $z > 0$.

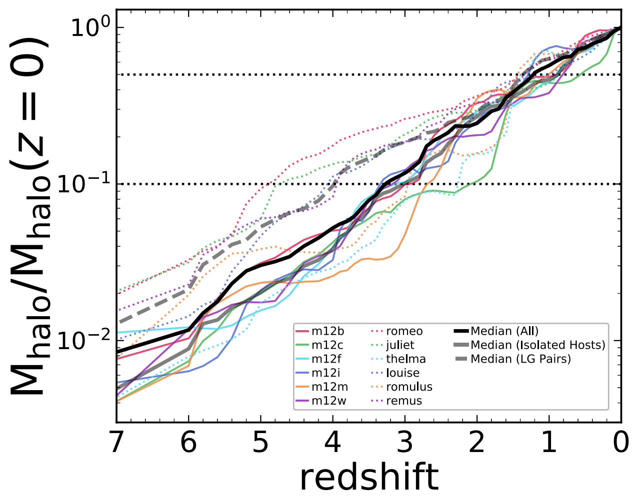

Figure 8. Similar to Fig. 2 (bottom left), but showing the *DM halo* mass of the MMP of each MW/M31-mass host, normalized to each host's M_{200m} at $z = 0$, as a function of redshift (bottom axis) or lookback time (top axis). We show the 6 isolated hosts (solid) and 6 LG-like paired hosts (dotted) in thin coloured lines, the median across all 12 hosts (thick solid black), and the medians for isolated (thick solid grey) and LG-like (thick dashed grey) hosts. The dotted horizontal lines show 10 and 50 per cent of the final mass. For the total median, the MMP halo reached 10 per cent of its final mass at $z \sim 3.3$ (11.8 Gyr ago). However, isolated hosts reached this later at $z \sim 3$ (11.6 Gyr ago), while LG-like hosts reached it earlier at $z \sim 4$ (12.2 Gyr ago). At later times ($z \lesssim 2$), the mass growth histories of isolated and LG-like hosts are more similar, so this environmental effect is weaker for later term growth. We conclude that this more rapid *halo* mass growth in denser proto-LG-like environments at early times likely drives the enhanced *stellar* mass growth in Fig. 2.

As mentioned in Section 2.1, the simulations assume flat ΛCDM cosmology, and the six cosmological parameters span a range of values that are consistent with Planck Collaboration VI (2018). However, not all simulations used the same cosmology, and one may wonder if this affects their formation times. These differences do not appear to correlate strongly with halo formation time. The Latte suite, Thelma and Louise, and Romulus and Remus adopt the most similar cosmologies. The most distinct cosmology, for Romeo and Juliet and m12w, includes both LG-like hosts and an isolated host, and although Romeo and Juliet did form the earliest (along with Romulus, with $z \sim 6$ for Romeo, $z \sim 5.3$ for Juliet and Romulus), m12w has a relatively late formation time ($z \sim 2.7$). Furthermore, Thelma and Louise span almost the entire range, with Thelma being the latest forming of all hosts and Louise being one of the earliest. Thus, we conclude that environment, and not slight differences in cosmology, is the primary cause of the difference in halo/galaxy formation history.

4 SUMMARY AND DISCUSSION

4.1 Summary

Using a suite of 12 FIRE-2 cosmological zoom-in simulations of MW/M31-mass galaxies, we explored their formation histories, to understand when a single main progenitor formed/emerged and quantify the hierarchical build-up from a progenitor population. We defined main progenitor formation in two ways: (1) when the growth of the MMP transitions from mostly *ex-situ* to *in-situ* star formation, and (2) by mass dominance (3:1 ratio or closer) of the MMP compared to other progenitors. The questions that we posed in the introduction and our corresponding answers are as follows:

(i) *What were the building blocks (progenitor galaxies) of MW/M31-mass galaxies, and how many were there across cosmic time?*

(a) About 100 progenitor galaxies with $M_{\rm star} \geq 10^5\,{\rm M}_\odot$, $\sim$10 with $M_{\rm star} \geq 10^7\,{\rm M}_\odot$, and $\sim$1 with $M_{\rm star} \geq 10^9\,{\rm M}_\odot$ formed a typical MW/M31-mass system. Thus, there were $\sim$5 times as many dwarf-galaxy progenitors with $M_{\rm star} > 10^5\,{\rm M}_\odot$ at $z \sim 4$–6 (12.2–12.8 Gyr ago) than survive to $z = 0$ (Fig. 3).

(b) The slope of the progenitor galaxy mass function was steeper with increasing redshift, which qualitatively agrees with observational and simulation results regarding the overall galaxy population (Fig. 3).

(c) At all redshifts, the *ex-situ* stellar mass of the accreted population was dominated by the few MMPs, and the *ex-situ* fraction monotonically increased with redshift (Fig. 4).

(ii) *When did the main progenitor of an MW/M31-mass galaxy form/emerge?*

(a) Across all 12 hosts, a single main progenitor typically formed/emerged around $z \approx 3.3$–3.5 (11.8–12.0 Gyr ago) (Figs 5–7).

(b) Stars in the inner bulge region formed in a single main progenitor earlier, typically at $z \approx 5.2$ (12.6 Gyr ago) across all 12 hosts (Fig. 5).

(c) Across all 12 hosts, the MMP reached 10 per cent of its present stellar mass by $z = 1.7$ (9.9 Gyr ago) and 50 per cent by $z = 0.5$ (5.1 Gyr ago). Thus, a single main progenitor typically formed/emerged when the host had only a few per cent of its final stellar mass (Fig. 2).

(iii) *Does the formation of MW/M31-mass galaxies depend on their environment, specifically, comparing isolated hosts to those in LG-like pairs?*

(a) LG-like hosts reached 10 and 50 per cent of their present stellar mass around $z = 2.4$ (11.0 Gyr ago) and $z = 0.8$ (6.9 Gyr ago), respectively. This was significantly earlier than when isolated hosts reached the same fractional masses: $z = 1.5$ (9.4 Gyr ago) for 10 per cent and $z = 0.5$ (5.1 Gyr ago) for 50 per cent (Fig. 2).

(b) Similarly, a single main progenitor of a typical LG-like paired host formed significantly earlier ($z_{\rm form} = 4.6$–4.9, $\sim$12.5 Gyr ago) than for a typical isolated host ($z_{\rm form} = 2.3$–2.7, 10.9–11.3 Gyr ago) (Figs 5–7). This is likely because their DM haloes formed earlier (Fig. 8).

(c) We find weaker differences between the overall progenitor galaxy populations for LG-like versus isolated hosts across time: The primary difference is that the number of progenitors peaked later for isolated hosts, reflecting their overall later formation histories (Fig. 3).

4.2 Discussion

Our simulations show that LG-like host galaxies were more massive than isolated hosts (of the same mass at $z \sim 0$), before $z \sim 2$, back to at least $z = 7$. This result is consistent with a related SFH-based analysis of the same simulations in Garrison-Kimmel et al. (2019b). As we showed in Section 3.6, this difference is reflected in the early formation histories of the DM host haloes, and it may be exacerbated in stellar mass growth if earlier halo formation promotes more metal production throughout the proto-volume, which would make gas cooling more efficient (Garrison-Kimmel et al. 2019b). That paper also found no difference in the SFHs of the satellite galaxies of FIRE-2 isolated versus LG-like hosts, but they *did* find differences in the formation times of central dwarf galaxies in the 'near-field' around LG-like versus isolated hosts, a population that we did not examine in this work.

Our results have key implications for studies of the early Universe and cosmic reionization. The slope of the galaxy luminosity (and mass) function at the faint (low-mass) end informs the contribution of low-mass galaxies to the ionizing flux during cosmic reionization at $z \gtrsim 7$. For example, if one naively extrapolates the slope to arbitrarily low mass, galaxies with an ultraviolet (UV) luminosity of $M_{\rm UV} \gtrsim -10$ generated most of the ionizing photons during reionization (∼50–80 per cent; Weisz & Boylan-Kolchin 2017). Thus, the evolution of the galaxy luminosity/mass function is of considerable interest. Several observational and theoretical works indicate that the slope of the faint end of the galaxy luminosity/mass function steepens with redshift (e.g. Bouwens et al. 2015; Song et al. 2016). For example, Bouwens et al. (2015) show that the faint-end slope of the UV luminosity function evolves from $\alpha \sim -1.64$ at $z \sim 4$ to $\alpha \sim -2.02$ at $z \sim 8$. Ma et al. (2018) show that in FIRE-2 simulations of larger populations of galaxies, the slope of the low-mass end of the stellar mass function decreases from $\alpha \sim -1.8$ at $z = 6$ to $\alpha \sim -2.13$ at $z = 12$. Graus et al. (2016) summarized several observational works and applied abundance matching to the DMO ELVIS simulations in order to calculate galaxy stellar mass and luminosity functions, finding a slight steepening of faint-end slope from $z = 2$ to 5.

It is not a priori obvious that the mass function of the progenitors of MW/M31-mass galaxies, which represent a biased region of all galaxies, reflects the overall galaxy population at a given redshift. This is an important question, because the faintest galaxies at $z \sim 7$ will be too faint even for direct JWST observations. Recent works have proposed using resolved stellar populations and SFHs of dwarf galaxies in the LG to infer the faint-end slope of the UV luminosity function at high redshifts, which already provides evidence for a break/rollover in the faint-end slope of the UV luminosity function at $z \sim 7$, given the number of UFD galaxies in the LG (Boylan-Kolchin, Bullock & Garrison-Kimmel 2014; Boylan-Kolchin et al. 2015; Weisz & Boylan-Kolchin 2017). On the one hand, our results in Fig. 3 (right) show that the progenitors of MW/M31-mass systems do show a similar steeping of mass-function slope to higher redshifts, which is at least qualitatively consistent with the overall galaxy population. However, our results also show that a significant fraction (∼80 per cent) of these progenitor dwarf galaxies have disrupted into the MW, which means that any inference from the LG population today is missing such progenitors in the early Universe. Thus, our results suggest that this 'near–far' approach remains promising, but more work is needed to explore quantitatively how representative the proto-LG environments were at high redshifts, which we plan to pursue in future work.

Wide-field surveys currently are measuring elemental abundances, ages, and phase-space distributions for millions of stars throughout all components of the MW, and their sampling rate is expected to continue to increase in the coming decade. A principle aim of these surveys is to reconstruct the formation history of the MW. Our analysis shows that MW/M31-like galaxies were assembled from ∼100 distinct dwarf galaxies with $M_{\rm star} \geq 10^5\,{\rm M}_{\odot}$, a majority of which merged by $z \sim 2$ (Fig. 3). Each of these dwarf galaxies had a unique orbit, and some likely had distinct elemental abundance patterns. In principle, it may be possible to identify members of many distinct progenitors by identifying them as clumps in a high-dimensional chemo-dynamic space (e.g. Ting, Conroy & Goodman 2015), even in the Solar neighbourhood (e.g. see recent work by Necib et al. 2019b). Achieving this in practice is challenging because progenitors that merged prior to $z \sim 3$ are likely thoroughly phase-mixed by $z = 0$ (see El-Badry et al. 2018b). Such phase-mixing of the earliest accreted progenitors occurs naturally during merging, and is likely exacerbated by stellar feedback-driven oscillations of the gravitational potential at early times (e.g. El-Badry et al. 2016).

On the other hand, progenitors accreted later ($z \lesssim 2$) – particularly the most massive ones – likely still can be identified. Indeed, there is already compelling evidence that much of the MW's inner stellar halo was formed by a single massive progenitor, whose stars remain dynamically coherent and chemically distinguishable (e.g. Belokurov et al. 2018; Helmi et al. 2018). This fact is not surprising in the context of our simulations: Because the progenitor mass functions of MW/M31-mass galaxies are relatively shallow (Fig. 3), our simulations generically predict that for any given formation redshift, most of the mass in the stellar halo was contributed by the few MMPs (Fig. 4). We finally note that this has also been seen in MW/M31-mass galaxies from the Illustris simulations (e.g. D'Souza & Bell 2018).

Populations of stars that are both old and metal poor tend to be more centrally concentrated despite the fact that the individual fractions of old or metal-poor stars increase with radius from the Galactic Centre (Starkenburg et al. 2017a; El-Badry et al. 2018b). However, because of continued star formation, central regions tend to get crowded over time and the fraction of old/metal-poor stars to the total stellar population becomes vanishingly small. Current stellar surveys (e.g. RAVE, GALAH, and APOGEE) thus have a better chance of detecting these stars outside of the solar circle (>8 kpc) and have already found a large number with [Fe/H] < -2. Despite this fact, APOGEE has observed ∼5100 stars near the Galactic bulge and have found a subset of these stars believed to be old, but more metal rich ([Fe/H] ~ -1; Schiavon et al. 2017). For future work, both within the MW and beyond, LSST also will be capable of finding RR Lyrae stars, which tend to be old (> 10 Gyr), within the LG volume (Oluseyi et al. 2012).

The formation times that we obtain for the entire galaxy (inner stellar halo + disc) are in line with those reported for the halo and thick disc in Gallart et al. (2019) ($z \sim$ 2–4.2, ∼10.5–12.3 Gyr ago). By analysing the difference in elemental abundances, they determined that the merger between Gaia-Enceladus/Sausage and the MW progenitor was about a 1:4 ratio, and took place roughly 10 Gyr ago, agreeing with previous work (e.g. Belokurov et al. 2018; Helmi et al. 2018; Nogueras-Lara et al. 2019), which would correspond to when the main galaxy was ∼10 per cent of its total stellar mass or ∼30 per cent of its total halo mass. Interestingly, around 10 Gyr, the M_2/M_1 ratios in the simulations are more pronounced, at a 1:10 ratio for the total sample, but closer for the isolated hosts, ∼1:4. Given that the work in Gallart et al. (2019) was done for an LG-like host (the MW itself), assuming that Gaia-Enceladus/Sausage was the second most massive component in the system at that time, our results suggest the ratio should be closer to 1:10 or 1:20. At these times, the thick disc was already in place, so this accretion event could have dynamically heated some of these stars into the halo, as well as provide a fresh reservoir of gas for further star formation.

Nogueras-Lara et al. (2019) estimated that the nuclear disc, embedded within the bulge, must have formed over 80 per cent of its stars more than 8 Gyr ago. They also claim that no significant merger >5:1 occurred in the MW within the last ∼10 Gyr. Using

CMDs of bulge stars to construct SFHs, other studies place the bulge at $\gtrsim$10 Gyr old, with no traces of a younger stellar population (Zoccali et al. 2003; Valenti et al. 2013; Barbuy et al. 2018; Renzini et al. 2018). Bernard et al. (2018) suggest that 50 per cent of these stars formed before ∼10 Gyr, and 80 per cent formed before ∼8 Gyr. The median formation times that we find for the inner bulge region are ∼2 Gyr earlier than the 10 Gyr lower limit; however, the scatter does span a wide range from ∼10 to 13 Gyr.

Kruijssen et al. (2019) inferred the MW's assembly history by combining the E-MOSAICS simulation suite, which models globular star cluster formation and evolution in MW/M31-mass galaxies, with the population of observed globular clusters around the MW. They estimate that the MW formed 50 per cent of its $M_{200m}(z = 0)$ around $z = 1.5$ (9.4 Gyr ago) comparable to both our results and that of Garrison-Kimmel et al. (2014). They also suggest that the main progenitor of the MW must have formed half of its stellar mass by $z \sim 1.2$ (8.6 Gyr ago) and that half of the stellar mass in the main galaxy at $z = 0$ formed *across all progenitors* by $z \sim 1.8$ (10.1 Gyr ago). By selecting globular cluster populations and inferring their evolution through age–metallicity space, Kruijssen et al. (2019) also estimated how many mergers of various masses occurred in the MW. They argue for ∼15 significant mergers throughout the MW's history, with a majority of them (∼9) happening before $z = 2$. Although we do not explicitly follow the halo merger tree in our analysis, we see rough consistency in that there were many more progenitor galaxies at high redshift, for all distance selections that we probe.

Although the formation times and mass functions derived in this paper are broadly consistent with other results in the literature, we recognize limitations in our analysis. First, we examine only 12 MW/M31-mass galaxies. A larger sample would allow us to probe better the distributions of formation times across a diverse set of formation histories. We also emphasize again that our galaxies, although comparable to the MW and M31 in many properties, were not created with the intention of exactly reproducing either galaxy. Therefore, one should not interpret the results in this work as necessarily applying exactly to the MW or M31, but rather as typical cosmological histories for MW/M31-mass galaxies. Finally, our results on stellar mass assembly are contingent on the accuracy and validity of the FIRE-2 model. For example, our assumed meta-galactic UV background from Faucher-Giguère et al. (2009) causes reionization to occur too early ($z \sim 10$) compared to recent observations (e.g. Planck Collaboration VI 2018, $z \sim 7$); similar results in some other simulation work have reported the same issue (e.g. Oñorbe, Hennawi & Lukić 2017).

In the future, an interesting follow-up analysis to our results would be a more thorough investigation into the importance of environment on formation time. Although we briefly discussed our initial reasoning of this difference in Section 3.6, more work is needed to provide a comprehensive explanation, including a more rigorous comparison of the merger trees between both isolated and LG-like hosts. The dependence of galaxy formation time on halo formation is likely only one piece of this story. Furthermore, there are other important factors that we did not investigate in our analysis, for example, 'patchy' reionization that likely did not happen instantaneously or spatially uniformly, as is implemented in FIRE simulations. Reionization heats gas and suppresses star formation, so a non-uniform reionization would shape a galaxy's SFH differently compared to our simulations (e.g. Lunnan et al. 2012; Zhu, Avestruz & Gnedin 2019). Patchy reionization also could have important consequences for the metal enrichment of gas and early forming Pop III stars. These first stars, and the feedback they produce within small, early forming progenitor galaxies, could affect the SFH of the main host at early times (e.g. Corlies, Johnston & Wise 2018; Koh & Wise 2018), and a proper implementation of their formation and evolution within simulations is critical. It also remains unclear exactly how Pop III stars enrich the ISM around them, and how they shape the formation of the subsequent generation of stars within the galaxy. Finally, the early formation period of galaxies is governed by many low-mass progenitors (e.g. Ciardi & Ferrara 2005; also see Fig. 1, left column), which are more sensitive to stellar feedback. It remains unclear how dusty these low-mass progenitors are and how that may affect both star formation and gas heating from the UV background. Galaxies that are more dusty can both better shield the reionizing photons and more effectively cool gas, which causes earlier star formation of lower mass stars than Pop III. Because we have not tested any of these additional points, it is unclear which, if any, would play the dominant role in determining a galaxy's formation time at such high redshifts.

We finally note two other studies focused on galactic archaeology within the FIRE simulation collaboration that are investigating the history and evolution of galaxies like the MW. One example is using chemical tagging of stars to infer where their birth environments were, as well as what other stars they may have co-formed with (Bellardini et al., in preparation). Another involves understanding where a population of metal-poor stars currently in the MW disc came from, as noted in Sestito et al. (2019) (Santistevan et al., in preparation).

ACKNOWLEDGEMENTS

The authors thank the anonymous referee for their helpful and thorough report. IBS, AW, and SB received support from NASA, through ATP grant 80NSSC18K1097 and *HST* grants GO-14734 and AR-15057 from STScI, the Heising-Simons Foundation, and a Hellman Fellowship. JBH acknowledges support from an ARC Laureate Fellowship. MBK acknowledges support from NSF grants AST-1517226, AST-1910346, and CAREER grant AST-1752913 and from NASA grants NNX17AG29G and *HST*-AR-14282, *HST*-AR-14554, *HST*-AR-15006, *HST*-GO-14191, and *HST*-GO-15658 from the Space Telescope Science Institute, which is operated by AURA, Inc., under NASA contract NAS5-26555. CAFG was supported by NSF through grants AST-1517491, AST-1715216, and CAREER award AST-1652522; by NASA through grant 17-ATP17-0067; and by a Cottrell Scholar Award from the Research Corporation for Science Advancement. We ran and analysed simulations using XSEDE supported by NSF grant ACI-1548562, Blue Waters via allocation PRAC NSF.1713353 supported by the NSF, and NASA HEC Program through the NAS Division at Ames Research Center. Some of this work was performed in part at KITP, supported by NSF grant PHY-1748958.

This work also used various python packages including NUMPY (van der Walt, Colbert & Varoquaux 2011), SCIPY (Virtanen et al. 2020), and MATPLOTLIB (Hunter 2007), as well as NASA's Astrophysics Data System.

DATA AVAILABILITY

Full simulation snapshots at $z = 0$ are available for m12i, m12f, and m12m at ananke.hub.yt. The python code used to analyse these data is available at https://bitbucket.org/isantis/progenitor, which uses the publicly available packages https://bitbucket.org/awetzel/gizmo_analysis, https://bitbucket.org/awetzel/halo_analysis, and https://bi tbucket.org/awetzel/utilities. Finally, data values in each figures are available at https://ibsantistevan.wixsite.com/mysite/publications.

REFERENCES

Anglés-Alcázar D., Faucher-Giguère C.-A., Kereš D., Hopkins P. F., Quataert E., Murray N., 2017, MNRAS, 470, 4698
Barbuy B., Chiappini C., Gerhard O., 2018, ARA&A, 56, 223
Behroozi P., Wechsler R. H., Hearin A. P., Conroy C., 2019, MNRAS, 488, 3143
Behroozi P. S., Wechsler R. H., Wu H.-Y., 2013a, ApJ, 762, 109
Behroozi P. S., Wechsler R. H., Wu H.-Y., Busha M. T., Klypin A. A., Primack J. R., 2013b, ApJ, 763, 18
Belokurov V., Erkal D., Evans N. W., Koposov S. E., Deason A. J., 2018, MNRAS, 478, 611
Bernard E. J., Schultheis M., Di Matteo P., Hill V., Haywood M., Calamida A., 2018, MNRAS, 477, 3507
Bland-Hawthorn J., Gerhard O., 2016, ARA&A, 54, 529
Bonaca A., Conroy C., Wetzel A., Hopkins P. F., Kereš D., 2017, ApJ, 845, 101
Bouwens R. J. et al., 2015, ApJ, 803, 34
Boylan-Kolchin M., Bullock J. S., Garrison-Kimmel S., 2014, MNRAS, 443, L44
Boylan-Kolchin M., Weisz D. R., Johnson B. D., Bullock J. S., Conroy C., Fitts A., 2015, MNRAS, 453, 1503
Brook C. B., Kawata D., Scannapieco E., Martel H., Gibson B. K., 2007, ApJ, 661, 10
Buck T., , Obreja A., Macciò A. V., Minchev I., Dutton A. A., Ostriker J. P., 2020, MNRAS, 491, 3461
Bullock J. S., Johnston K. V., 2005, ApJ, 635, 931
Bullock J. S., Kravtsov A. V., Weinberg D. H., 2001, ApJ, 548, 33
Carlesi E., Hoffman Y., Gottlöber S., Libeskind N. I., Knebe A., Yepes G., Pilipenko S. V., 2020, MNRAS, 491, 1531
Chaplin W. J. et al., 2014, ApJS, 210, 1
Chiaki G., Wise J. H., 2019, MNRAS, 482, 3933
Ciardi B., Ferrara A., 2005, Space Sci. Rev., 116, 625
Cooper A. P. et al., 2010, MNRAS, 406, 744
Corlies L., Johnston K. V., Wise J. H., 2018, MNRAS, 475, 4868
Creevey O. L. et al., 2017, A&A, 601, A67
Danieli S., van Dokkum P., Merritt A., Abraham R., Zhang J., Karachentsev I. D., Makarova L. N., 2017, ApJ, 837, 136
Deason A. J., Mao Y.-Y., Wechsler R. H., 2016, ApJ, 821, 5
de Bennassuti M., Schneider R., Valiante R., Salvadori S., 2014, MNRAS, 445, 3039
de Bennassuti M., Salvadori S., Schneider R., Valiante R., Omukai K., 2017, MNRAS, 465, 926
De Silva G. M. et al., 2015, MNRAS, 449, 2604
Dixon K. L., Iliev I. T., Gottlöber S., Yepes G., Knebe A., Libeskind N., Hoffman Y., 2018, MNRAS, 477, 867
D'Souza R., Bell E. F., 2018, MNRAS, 474, 5300
Eggen O. J., Lynden-Bell D., Sandage A. R., 1962, ApJ, 136, 748
El-Badry K., Wetzel A., Geha M., Hopkins P. F., Kereš D., Chan T. K., Faucher-Giguère C.-A., 2016, ApJ, 820, 131
El-Badry K. et al., 2018a, MNRAS, 473, 1930
El-Badry K. et al., 2018b, MNRAS, 480, 652
Escala I. et al., 2018, MNRAS, 474, 2194
Fall S. M., Efstathiou G., 1980, MNRAS, 193, 189
Faucher-Giguère C.-A., Lidz A., Zaldarriaga M., Hernquist L., 2009, ApJ, 703, 1416
Forero-Romero J. E., Hoffman Y., Yepes G., Gottlöber S., Piontek R., Klypin A., Steinmetz M., 2011, MNRAS, 417, 1434
Freeman K., Bland-Hawthorn J., 2002, ARA&A, 40, 487
Gaia Collaboration, 2018, A&A, 616, A1
Gallart C. et al., 2015, ApJ, 811, L18
Gallart C., Bernard E. J., Brook C. B., Ruiz-Lara T., Cassisi S., Hill V., Monelli M., 2019, Nat. Astron., 3, 932
Garrison-Kimmel S., Boylan-Kolchin M., Bullock J. S., Lee K., 2014, MNRAS, 438, 2578
Garrison-Kimmel S. et al., 2017, MNRAS, 471, 1709
Garrison-Kimmel S. et al., 2018, MNRAS, 481, 4133
Garrison-Kimmel S. et al., 2019a, MNRAS, 487, 1380
Garrison-Kimmel S. et al., 2019b, MNRAS, 489, 4574
Geha M. et al., 2017, ApJ, 847, 4
Ge Z. S., Bi S. L., Chen Y. Q., Li T. D., Zhao J. K., Liu K., Ferguson J. W., Wu Y. Q., 2016, ApJ, 833, 161
Grand R. J. J. et al., 2017, MNRAS, 467, 179
Graus A. S., Bullock J. S., Boylan-Kolchin M., Weisz D. R., 2016, MNRAS, 456, 477
Graziani L., Salvadori S., Schneider R., Kawata D., de Bennassuti M., Maselli A., 2015, MNRAS, 449, 3137
Graziani L., de Bennassuti M., Schneider R., Kawata D., Salvadori S., 2017, MNRAS, 469, 1101
Griffen B. F., Ji A. P., Dooley G. A., Gómez F. A., Vogelsberger M., O'Shea B. W., Frebel A., 2016, ApJ, 818, 10
Griffen B. F., Dooley G. A., Ji A. P., O'Shea B. W., Gómez F. A., Frebel A., 2018, MNRAS, 474, 443
Guedes J., Callegari S., Madau P., Mayer L., 2011, ApJ, 742, 76
Hahn O., Abel T., 2011, MNRAS, 415, 2101
Hawkins K., Jofré P., Gilmore G., Masseron T., 2014, MNRAS, 445, 2575
Helmi A., 2008, A&AR, 15, 145
Helmi A., Babusiaux C., Koppelman H. H., Massari D., Veljanoski J., Brown A. G. A., 2018, Nature, 563, 85
Hill A. R., Muzzin A., Franx M., Marchesini D., 2017, ApJ, 849, L26
Hopkins P. F., 2009, in Jogee S., Marinova I., Hao L., Blanc G. A., eds, ASP Conf. Ser. Vol. 419, Galaxy Evolution: Emerging Insights and Future Challenges. Astron. Soc. Pac., San Francisco, p. 228
Hopkins P. F., 2015, MNRAS, 450, 53
Hopkins P. F., 2016, MNRAS, 455, 89
Hopkins P. F., Hernquist L., Martini P., Cox T. J., Robertson B., Di Matteo T., Springel V., 2005, ApJ, 625, L71
Hopkins P. F. et al., 2018, MNRAS, 480, 800
Hunter J. D., 2007, Comput. Sci. Eng., 9, 90
Johnston K. V., Bullock J. S., Sharma S., Font A., Robertson B. E., Leitner S. N., 2008, ApJ, 689, 936
Karachentsev I. D., Kudrya Y. N., 2014, AJ, 148, 50
Koh D., Wise J. H., 2018, MNRAS, 474, 3817
Kourkchi E., Tully R. B., 2017, ApJ, 843, 16
Kroupa P., 2001, MNRAS, 322, 231
Kruijssen J. M. D., Pfeffer J. L., Reina-Campos M., Crain R. A., Bastian N., 2019, MNRAS, 486, 3180
Krumholz M. R., Gnedin N. Y., 2011, ApJ, 729, 36
Leitherer C. et al., 1999, ApJS, 123, 3
Leitner S. N., 2012, ApJ, 745, 149
Li H.-N., Zhao G., Christlieb N., Wang L., Wang W., Zhang Y., Hou Y., Yuan H., 2015, ApJ, 798, 110
Lunnan R., Vogelsberger M., Frebel A., Hernquist L., Lidz A., Boylan-Kolchin M., 2012, ApJ, 746, 109
Magg M., Hartwig T., Agarwal B., Frebel A., Glover S. C. O., Griffen B. F., Klessen R. S., 2018, MNRAS, 473, 5308
Majewski S. R., Skrutskie M. F., Weinberg M. D., Ostheimer J. C., 2003, ApJ, 599, 1082
Majewski S. R. et al., 2017, AJ, 154, 94
Martig M. et al., 2016, MNRAS, 456, 3655
Ma X., Hopkins P. F., Wetzel A. R., Kirby E. N., Anglés-Alcázar D., Faucher-Giguère C.-A., Kereš D., Quataert E., 2017, MNRAS, 467, 2430
Ma X. et al., 2018, MNRAS, 478, 1694
Miglio A. et al., 2017, Astron. Nachr., 338, 644
Mo H. J., Mao S., White S. D. M., 1998, MNRAS, 295, 319
Monachesi A. et al., 2019, MNRAS, 485, 2589
Müller O., Rejkuba M., Pawlowski M. S., Ibata R., Lelli F., Hilker M., Jerjen H., 2019, A&A, 629, A18
Necib L., Lisanti M., Garrison-Kimmel S., Wetzel A., Sanderson R., Hopkins P. F., Faucher-Giguère C.-A., Kereš D., 2019a, ApJ, 883, 27

Necib L. et al., 2019b, preprint (arXiv:1907.07190)
Newberg H. J. et al., 2002, ApJ, 569, 245
Nogueras-Lara F. et al., 2020, Nature Astronomy, 4, 377
Oluseyi H. M. et al., 2012, AJ, 144, 9
Ostriker J. P., Tremaine S. D., 1975, ApJ, 202, L113
Oñorbe J., Garrison-Kimmel S., Maller A. H., Bullock J. S., Rocha M., Hahn O., 2014, MNRAS, 437, 1894
Oñorbe J., Hennawi J. F., Lukić Z., 2017, ApJ, 837, 106
Papovich C. et al., 2015, ApJ, 803, 26
Planck Collaboration VI, 2018, preprint (arXiv:1807.06209)
Rees M. J., Ostriker J. P., 1977, MNRAS, 179, 541
Renzini A. et al., 2018, ApJ, 863, 16
Riebe K. et al., 2013, Astron. Nachr., 334, 691
Robertson B., Bullock J. S., Cox T. J., Di Matteo T., Hernquist L., Springel V., Yoshida N., 2006, ApJ, 645, 986
Safarzadeh M., Ji A. P., Dooley G. A., Frebel A., Scannapieco E., Gómez F. A., O'Shea B. W., 2018, MNRAS, 476, 5006
Salvadori S., Schneider R., Ferrara A., 2007, MNRAS, 381, 647
Samuel J. et al., 2020, MNRAS, 491, 1471
Sanderson R. E. et al., 2018, ApJ, 869, 12
Sanderson R. E. et al., 2020, ApJS, 246, 6
Sawala T. et al., 2016, MNRAS, 457, 1931
Scannapieco E., Kawata D., Brook C. B., Schneider R., Ferrara A., Gibson B. K., 2006, ApJ, 653, 285
Schiavon R. P. et al., 2017, MNRAS, 465, 501
Schuster W. J., Moreno E., Nissen P. E., Pichardo B., 2012, A&A, 538, A21
Searle L., Zinn R., 1978, ApJ, 225, 357
Sestito F. et al., 2019, MNRAS, 484, 2166
Silva Aguirre V. et al., 2018, MNRAS, 475, 5487
Smercina A., Bell E. F., Price P. A., D'Souza R., Slater C. T., Bailin J., Monachesi A., Nidever D., 2018, ApJ, 863, 152
Song M. et al., 2016, ApJ, 825, 5
Springel V., Hernquist L., 2005, ApJ, 622, L9
Starkenburg E., Oman K. A., Navarro J. F., Crain R. A., Fattahi A., Frenk C. S., Sawala T., Schaye J., 2017a, MNRAS, 465, 2212
Starkenburg E. et al., 2017b, MNRAS, 471, 2587
Steinmetz M. et al., 2006, AJ, 132, 1645
Stewart K. R., Bullock J. S., Wechsler R. H., Maller A. H., Zentner A. R., 2008, ApJ, 683, 597
Su K.-Y., Hopkins P. F., Hayward C. C., Faucher-Giguère C.-A., Kereš D., Ma X., Robles V. H., 2017, MNRAS, 471, 144
Ting Y.-S., Conroy C., Goodman A., 2015, ApJ, 807, 104
Valenti E., Zoccali M., Renzini A., Brown T. M., Gonzalez O. A., Minniti D., Debattista V. P., Mayer L., 2013, A&A, 559, A98
van der Walt S., Colbert S. C., Varoquaux G., 2011, Comput. Sci. Eng., 13, 22
van Dokkum P. G. et al., 2013, ApJ, 771, L35
Virtanen P. et al., 2020, Nat. Methods, 17, 261
Weisz D. R., Boylan-Kolchin M., 2017, MNRAS, 469, L83
Wetzel A. R., Hopkins P. F., Kim J.-h., Faucher-Giguère C.-A., Kereš D., Quataert E., 2016, ApJ, 827, L23
White S. D. M., Rees M. J., 1978, MNRAS, 183, 341
Yuan Z. et al., 2020, ApJ, 891, 39
Yu S. et al., 2020, MNRAS, 494, 1539
Zhu H., Avestruz C., Gnedin N. Y., 2019, ApJ, 882, 152
Zoccali M. et al., 2003, A&A, 399, 931

This paper has been typeset from a TEX/LATEX file prepared by the author.